DUDLEY KNOX LIBRARY
NAVAL POSTGRADUATE SCHOOL
MONTEREY, CALIFORNIA 93943-5002

NAVAL POSTGRADUATE SCHOOL
Monterey, California

THESIS

M4855

ATOMIC RELAXATION AND VACANCY-INTERSTITIAL RECOMBINATION IN Zr AND Zr_3Al

by

Vito Michael Menzella

December 1988

Thesis Advisor: Roger Smith
Co-Advisor: Dora F. Pedraza

Approved for public release; distribution is unlimited

T242179

DEPARTMENT OF THE NAVY COPIER AT GOVERNMENT

REPORT DOCUMENTATION PAGE

PORT SECURITY CLASSIFICATION nclassified	1b RESTRICTIVE MARKINGS
CURITY CLASSIFICATION AUTHORITY	3 DISTRIBUTION / AVAILABILITY OF REPORT Approved for public release; distribution is unlimited
CLASSIFICATION / DOWNGRADING SCHEDULE	
FORMING ORGANIZATION REPORT NUMBER(S)	5 MONITORING ORGANIZATION REPORT NUMBER(S)
AME OF PERFORMING ORGANIZATION l Postgraduate School — 6b OFFICE SYMBOL (If applicable): Code 61	7a NAME OF MONITORING ORGANIZATION Naval Postgraduate School
DRESS (City, State, and ZIP Code) nterey, CA 93943-5000	7b ADDRESS (City, State, and ZIP Code) Monterey, CA 93943-5000
AME OF FUNDING / SPONSORING GANIZATION — 8b OFFICE SYMBOL (If applicable)	9 PROCUREMENT INSTRUMENT IDENTIFICATION NUMBER
DRESS (City, State, and ZIP Code)	10 SOURCE OF FUNDING NUMBERS PROGRAM ELEMENT NO | PROJECT NO | TASK NO | WORK UNIT ACCESSION NO

TLE (Include Security Classification)

TOMIC RELAXATION AND VACANCY-INTERSTITIAL RECOMBINATION IN Zr AND Zr_3Al

RSONAL AUTHOR(S)
Menzella, Vito M.

YPE OF REPORT	13b TIME COVERED	14 DATE OF REPORT (Year, Month, Day)	15 PAGE COUNT
ter's Thesis	FROM _____ TO _____	December 1988	96

PPLEMENTARY NOTATION The views expressed in this thesis are those of the author and do not flect the official policy or position of the Department of Defense or the U.S.Government

COSATI CODES			18 SUBJECT TERMS (Continue on reverse if necessary and identify by block number)
ELD	GROUP	SUB-GROUP	Molecular Dynamics of Vacancies Atomic Configurations Recombination

BSTRACT (Continue on reverse if necessary and identify by block number)

This thesis examines two problems associated with crystalline defects in the materials and Zr_3Al, by means of a molecular dynamics simulation.

In the first problem, the relaxed configuration around a single vacancy, a di-vacancy l a tri-vacancy is computed by introducing the defect into a perfect lattice and namically relaxing the crystal until it attains equilibrium. The results are in litative agreement with "static" studies but show clearly that first and second ghbors have different relaxed states depending on their configuration in the initial stal lattice.

The recombination studies show that a vacancy-interstitial pair quickly relaxes to perfect crystal if the interstitial is within an adjacent crystalline cell.

ISTRIBUTION / AVAILABILITY OF ABSTRACT UNCLASSIFIED/UNLIMITED ☐ SAME AS RPT ☐ DTIC USERS	21 ABSTRACT SECURITY CLASSIFICATION Unclassified
NAME OF RESPONSIBLE INDIVIDUAL Roger Smith	22b TELEPHONE (Include Area Code) (408) 646-2697 — 22c OFFICE SYMBOL Code 61SM

ORM 1473, 84 MAR — 83 APR edition may be used until exhausted; All other editions are obsolete

SECURITY CLASSIFICATION OF THIS PAGE

☆ U.S. Government Printing Office 1986—606-243

Approved for public release; distribution is unlimited.

Atomic Relaxation and Vacancy-Interstitial Recombination in Zr and Zr_3Al

by

Vito Michael Menzella
Lieutenant, United States Navy
B.A., Rutgers College, 1981

Submitted in partial fulfillment of the
requirements for the degree of

MASTER OF SCIENCE IN PHYSICS

from the

NAVAL POSTGRADUATE SCHOOL
DECEMBER 1988

ABSTRACT

This thesis examines two problems associated with crystalline defects in the materials Zr and Zr_3Al, by means of a molecular dynamics computer simulation.

In the first problem, the relaxed configuration around a single vacancy, a di-vacancy and a tri-vacancy is computed by introducing the defect into a perfect lattice and dynamically relaxing the crystal until it attains equilibrium. The results are in qualitative agreement with "static" studies but show clearly that first and second neighbors have different relaxed states depending on their configuration in the initial crystal lattice.

The recombination studies show that a vacancy-interstitial pair quickly relaxes to the perfect crystal if the interstitial is within an adjacent crystalline cell.

Thesis
M4855
C.1

TABLE OF CONTENTS

I. BACKGROUND 1

A. INTRODUCTION. 1

B. HISTORICAL OVERVIEW 2

C. PHYSICAL BACKGROUND 5

D. COMPUTER SIMULATION 8

E. APPLICATIONS 9

II. OBJECTIVES 11

A. THESIS OBJECTIVES 11

B. PREVIOUS EFFORTS 12

C. A DYNAMIC SIMULATION 13

III. COMPUTER SIMULATION AND MODEL DEVELOPMENT 16

A. THE COMPUTER MODEL AND RELATED PROGRAMS 16

1. BCT 16

2. Ancillary Programs 18

a. INTEG 19

b. POTVEC 19

c. POTIN and POTFN(K) 19

d. BCT001 19

e. HALLOY 19

B. PROPERTIES OF Zr AND Zr_3Al 20

C. POTENTIAL FUNCTIONS 20

1. Basics 20

a. Moliere 21

SCHOOL,
MONTEREY, CALIFORNIA 93943-5002

b. Morse 22

c. Composite Morse-Moliere 23

2. Selection of Potential Function Parameters 23

IV. RESULTS 24

A. RELAXED ATOMIC CONFIGURATIONS 24

1. General 24

2. Single Vacancy Results 25

3. Di-Vacancy Results 27

4. Tri-Vacancy Results 30

5. Atomic Oscillations 33

B. RECOMBINATION STUDIES 34

1. Lattice Orientations and Terminology . . . 34

2. Trial Description 35

3. Recombination Results 36

a. Momentum Direction 36

b. Orientation 38

c. Electronic Energy Losses 39

d. Alloy 40

V. CONCLUSIONS AND RECOMMENDATIONS 42

APPENDIX A - TABLES 44

APPENDIX B - FIGURES 52

LIST OF REFERENCES 86

INITIAL DISTRIBUTION LIST 89

ACKNOWLEDGMENT

I would like to express my appreciation to the late Professor Don Harrison of the United States Naval Postgraduate School. He introduced me to computer programming and computer simulation, and provided me with the necessary guidance during the early portions of my studies. Without his help and deep concern for my early comprehension of the model, I would not have been able to complete my thesis. I humbly thank him for all of his support.

I would also like to thank my thesis advisors, Roger Smith and Dora Pedraza, for all of their patience and time. They put aside their own work to promptly answer all of my questions, and for this I am truly grateful.

I. BACKGROUND

A. INTRODUCTION

When a solid is exposed to energetic particles, point defects can be produced in the crystal lattice of the material. These point defects can be of various types, such as interstitials, substitutional impurities, and vacancies. These point defects can interact, and possibly alter the properties of the material. This study focuses on a molecular dynamics study of vacancies and interstitials in the ordered intermetallic compound Zr_3Al. This alloy has been analyzed in the late 70's and early 80's for its possible use as a material for pressure tubes in nuclear reactors [Ref. 1]. Therefore, studies on the radiation damage events and the associated radiation effects on the alloy are of particular interest.

It is important to point out the difference between radiation damage and radiation effects. Radiation damage is the term applied to the **microscopic** events produced by energetic particles which irradiate a material. For example, a fast neutron may collide with a lattice atom and knock it out of the lattice, thereby creating a vacancy. The displaced atom may take up a position in the lattice that is not a regular lattice site. This atom is then termed an interstitial. Radiation effects are the **macroscopic** changes

of the solid produced as a result of irradiation by energetic particles. The radiation damage process is very fast, and temperature independent since the event occurs at energies much larger than thermal energies [Ref. 2]. Radiation effects are temperature dependent, and take a long time to be observed. For example, the irradiation of reactor fuel elements results in the hardening of the component metals or alloys, which leads to an increase in yield strength, but a decrease in ductility [Ref. 3]. Under abnormal conditions, this property change may be deleterious. However, it is only a concern after many hours of reactor operation.

B. HISTORICAL OVERVIEW

One of the first studies of the importance of radiation effects in solids has its origin in the work begun in 1942 at the Metallurgical Laboratories of the Manhattan District in Chicago. This laboratory had the task of developing large scale reactors which could produce weapons grade plutonium. In the middle of 1942, Spedding and Teller [Ref. 4] predicted that the high radiation flux generated from the operation of large reactors could produce changes in the mechanical properties of reactor materials.

In 1942, Wigner [Ref. 5] did a theoretical study of the effects of a large, fast neutron flux on the properties of reactor fuel elements. Looking at the fraction of atoms displaced from their normal lattice sites in the graphite moderator, he concluded that the effects of radiation damage

could not be ignored in the design and operation of large scale reactors. From these studies and others, physicists and engineers working on the Hanford reactor design were able to predict what would happen to the solid components of the reactor fuel elements and moderator [Ref. 4].

The pioneers in nuclear engineering were not alone in studying the effects of radiation damage in solids. The irradiation of semi-conductors was also of interest since the performance of semi-conductors can be adversely affected under bombardment by protons, neutrons, gamma rays and electrons. In 1950, Brattain and Pearson [Ref. 6] at Bell Laboratories bombarded n-type germanium with alpha particles from polonium. A thin slab of material was bombarded on one side and the conductance normal to the bombarding direction was measured as a function of time. It was observed that the conductance of germanium was significantly affected under irradiation by alpha particles, to the extent that germanium converted from n-type to p-type at the minimum conductance point.

Early theories on the mechanism of radiation damage in solids were concerned with the production of primary knock-on atoms (PKA). In the case of neutron bombardment, the highly energetic incident particle undergoes elastic or inelastic collisions with the atoms of the "target" material, whereby the incident particle transfers enough energy to the target atom to free it from its crystal lattice site. This target

atom is called the primary knock-on atom, and it can be charged, which can lead to the following:

1. Ionization or excitation of electrons in the crystal.
2. The primary knock-on atom can collide with other lattice atoms to produce secondary knock-on atoms, which are freed from their lattice sites, but with a kinetic energy lower than the primary knock-on atom.
3. The transmission of energy to neighboring lattice atoms in an amount which can thermally excite the atom, but not enough so as to remove it from its crystal lattice site.

The third possibility was termed a "thermal spike," since the effect of the energy transfer was analogous to instantaneously raising the temperature of the atom. In 1949 Siegel showed the effects of this thermal spike on the order in the alloy Cu_3Au [Ref. 7]. Siegel showed that the irradiation of a solid by the neutron flux in a reactor can produce displaced atoms, lattice vacancies, localized thermal lattice vibrations, and foreign atoms, all of which can affect the macroscopic properties of the alloy.

These early studies coupled with advances in the fields of solid state physics and metallurgy led to more modern theories of the mechanism of radiation damage. These theories are based upon the defects present in crystal structures, which are formed under irradiation conditions. By studying how the defects move and aggregate in the solid, a more accurate description of the mechanism of radiation damage and subsequent radiation effects can be obtained. For example, in 1978, Howe and Rainville [Ref. 8] bombarded

Zr_3Al, an ordered intermetallic compound, with Ar^+,N^+, and Cu^+ ions, and observed the irradiation-induced transition sequence ordered → disordered → amorphous state. The irradiation-induced crystalline to amorphous transition in ordered intermetallic compounds is a widely known phenomenon, and much effort is being devoted to understand the mechanism of this transition [Ref. 9-10]. Thus, it is particularly important to understand the point defect configuration in these materials.

C. PHYSICAL BACKGROUND

Radiation damage can be defined as the spatial distribution of point defects which remains after a solid is irradiated. Radiation effects are the macroscopically observable changes in the properties and structural features of the solid after irradiation of the material. The earliest theory of radiation damage was based on a collision theory. In this theory, a highly energetic bombarding particle, for example a neutron of energy >0.1MeV, collides with the nucleus of an atom in the crystal lattice of the target material, and the collision results in a transfer of kinetic energy to the atom. If the energy transferred is greater than the binding energy of the atom in its lattice position, the atom will be knocked out of its lattice site and move through the crystal. This PKA has an energy on the order of tens to hundreds of keV [Ref. 11]. The motion of the PKA away from its original lattice site results in a vacancy.

The PKA will in turn collide with other atoms in the crystal lattice and possibly displace other atoms from their original lattice sites. Therefore, a cascade of atomic collisions is the result of a single bombardment event. The displaced atoms ultimately appear as interstitial atoms in the lattice. A complex type of interstitial is one in the dumbbell configuration, which is achieved when two atoms share one lattice site. This configuration has been described and studied by many researchers [Ref. 12-13]. In summary, a single bombarding event produces an ensemble of point defects in the crystal. The subsequent behavior of point defects, that is whether they aggregate, annihilate in the material, or are retained, ultimately gives rise to changes in the physical properties of the crystal.

Theoretical approaches to the study of radiation effects can involve the concept of a cascade of point defects in the crystal. The studies of displacement cascades depend critically on the interatomic forces and potentials present. In the most simplistic approach, the cascade is the result of independent, two-body collisions between the PKA's and atoms in lattice sites. Knock-on atoms are then assumed to move freely between collisions [Ref. 14]. This is known as the binary collision approximation. A more advanced approach to the study of radiation effects is by computer simulations [Ref. 15], which take into account not only more realistic

interatomic forces, but also multiple interactions. This is known as molecular dynamics and is the approach used here.

It has been found that the type of radiation damage observed depends on the material, irradiation temperature, and the nature of the irradiating particle. One property of materials which is of interest in the nuclear engineering field is the amorphization of solids, and under given irradiation conditions, whether or not a material will undergo amorphization.

Amorphization of a crystal is the loss of translational symmetry. Some ordered intermetallic compounds which possess regular atomic arrangements, a characteristic of a crystal, can undergo amorphization when irradiated. Subsequent heating above a certain temperature allows the amorphous alloy to crystallize, and radiation damage will have been annealed. Annealing is a heat treatment commonly used to eliminate structural defects in a metal or to induce phase transformations. Table A1 gives some examples of ordered intermetallic alloys. The ordered intermetallic alloy Zr_3Al has been a candidate material for use in nuclear reactors because of its low thermal neutron cross section and its good tensile properties in the unirradiated state [Ref. 1]. Understanding the alloy's performance in the irradiated state is thus of technical importance.

In 1949, Siegel [Ref. 7] observed that irradiation of the ordered alloy Cu_3Au can induce the loss of chemical long

range order if the temperature of the alloy is kept under 200°C, but not amorphization. The ordered → disordered transition was manifested by a reduction in the resistivity of an ordered sample after irradiation by fast neutrons to a fluence of $3.3*10^{19}$ N/cm^2 at 40°C. By contrast, in 1978, Howe and Rainville [Ref. 16] studied the effects of ion bombardment on Zr_3Al. They found that long range order was lost. Also, they reported the gradual amorphization of the alloy with increasing dose at a rate which depended on the temperature of irradiation.

As previously stated, the point defect configurations constitute a step of primary importance in the understanding of radiation effects such as amorphization. The reason why these configurations are important is because current theories of amorphization mechanisms are based upon the assumption that a build up of irradiation induced point defects is what causes destabilization of the crystalline lattice and its collapse to an amorphous state [Ref. 17].

D. COMPUTER SIMULATION

In 1960, Gibson, Goland, Milgram and Vineyard [Ref. 15] used a computer simulation to study radiation damage in copper. They studied radiation damage events up to energies of 400 eV. The code generated the copper lattice and simulated the effects of knock-on atoms produced by irradiation. This was the first use of a computer simulation for the purpose of studying radiation damage in materials.

One of the first attempts at an analytical theory was in 1954, when Huntington [Ref. 18] developed a theoretical study of the radiation damage in FCC metals. One limitation of current analytic theory is that the radiation damage process is considered as a cascade of hard-sphere, independent collisions. Computer simulations allow one to take into account the many-body features of the radiation damage process. The high-speed of the computer coupled with its large memory allows the characterization of each target atom by its mass, interatomic potential, position and velocity. This allows Newton's laws to be solved numerically, as is done in the multiple interaction (MI) time-step model used in this thesis. The MI code used in this thesis is BCT001, which is a full-lattice simulation developed at the Naval Postgraduate School.

E. APPLICATIONS

The study of radiation damage in materials is useful for several reasons. It is of fundamental importance with regard to the technological industries of nuclear engineering and space exploration, but it is also important in the production of microelectronic devices. Here materials undergo controlled changes after bombardment by ion beams. Ion implantation is a controlled technique used in semiconductor manufacture.

Intermetallic phase precipitates in the Zircaloys are known to become amorphous after prolonged irradiation [Ref. 19]. Zircaloys are very widely used in the nuclear industry. No studies are as yet available on the effects of these changes on the mechanical properties of the alloys or on the limitations to their use as a function of dose. The Zircaloy matrix undergoes one particular radiation effect known as irradiation growth, a dimensional change which limits its useful life in a reactor environment [Ref. 20].

The exposure of semi-conductor components present in space systems also makes a study of radiation damage in materials important. The fluxes of various types of radiations which impinge upon the components of satellites or manned vehicles can produce harmful effects on semi-conductor components. By studying the mechanism of radiation damage in semi-conductor components, it may then be possible to develop methods, such as the use of shielding, to counter the harmful effects of radiation on critical components.

II. OBJECTIVES

A. THESIS OBJECTIVES

This thesis is part of a research collaboration program initiated by the late Professor D.E. Harrison of the Naval Postgraduate School and Dr. D.F. Pedraza of the Oak Ridge National Laboratory. The goal of the program is to simulate the irradiation-induced crystalline to amorphous transition in intermetallic compounds, assuming a mechanism of defect buildup. One defect of interest is a vacancy-interstitial coupled pair, as described in several papers [Ref. 9-10].

In the context of that program, it is first necessary to study the relaxed atomic configurations around a vacancy and around a cluster of vacancies, as well as the atomic displacements involved and the energy of the defects. Second, it is necessary to calculate self-interstitial configurations, single as well as clusters. Important computations include atomic displacements around single and clustered self-interstitials, and the corresponding energies and formation volumes. Third, it is necessary to calculate the vacancy-interstitial spontaneous recombination distance as a function of the self-interstitial orientation. The orientation of concern is the dumbbell configuration, with the distance mentioned above measured relative to the vacancy. This study will deal with the first and third problems.

B. PREVIOUS EFFORTS

Although there has been extensive work reported on the simulation of point defect configurations and the displacement field around them, most has been done using a static lattice approach [Ref. 21]. In this approach, the defect is "moved" into different positions until the potential energy of the lattice reaches a minimum. Although there have also been molecular dynamics simulations of point defects, most studies use "static" approaches, where a minimum of the lattice potential energy is sought, irrespective of the dynamics by which that minimum can be achieved. In these cases, the simulation progresses until the total force acting on every atom of the crystallite is zero. A few studies involving the use of such methods are described below.

In 1968, Englert, Tompa and Bullough [Ref. 22] studied point defects and dislocations in copper. They developed a pair potential for copper which was used to study the atomic configurations of various line and point defects in the metal. A crystallite containing the defect of interest was simulated, for FCC copper. The crystallite was allowed to find its minimum potential energy configuration via a relaxation procedure known as the conjugate gradient technique [Ref. 23]. This technique involves the evaluation of the first derivative of the potential, the force, and is designed to guarantee the convergence of the potential energy

to a minimum energy. They found that the minimum energy atomic configuration under conditions of a single vacancy corresponded to 1.09eV. This was in good agreement with the experimental value of 1.14eV. They also computed the atomic displacement field around the vacancy, up to the seventh nearest neighbor, which is contained in Table A2.

In 1974, Savino and Perrin [Ref. 24] studied the morphology of planar vacancy aggregates in copper. The computer simulation created a FCC lattice with the vacancy defect of interest, and the method of conjugate gradients was used to obtain the equilibrium energy configuration. This study found that six vacancies collapsed to form either loops or stacking fault tetrahedra.

The method of conjugate gradients has also been used to study the effects of interstitials on the atomic configuration and energies in FCC metals. In 1976 Schober [Ref. 13] studied single and multiple interstitials in copper, using the computer program DEVIL developed in AERE Harwell. Computed values included the atomic displacements and relaxation volumes for various defect configurations. Various results are shown in Table A3. Single and multiple interstitials were found to be highly mobile, in that the activation energies for migration of the defect are low.

C. A DYNAMIC SIMULATION

The studies above are "static" approaches, since a minimum potential energy of the lattice was sought. The

simulation is carried out until the total force acting on every atom in the crystal is zero. In this thesis, a fully dynamic simulation is attempted. The defect is introduced into the crystallite, resulting in a perturbed crystal. As the simulation progresses, the perturbation decays and the atoms are displaced to positions in which they are fairly stable.

For the relaxed vacancy studies, the perturbation involves removing one or several atoms from their normal lattice sites. The atomic displacements of surrounding atoms are then computed. For the studies of vacancy-interstitial recombination, the perturbation involves placing an interstitial in the dumbbell configuration in a crystal lattice, with a corresponding vacancy. One atom of the dumbbell is given a kinetic energy, and this perturbation and its effects on the lattice are be studied. Of concern is the spontaneous recombination distance as a function of the dumbbell orientation relative to the vacancy.

Most simulations of point defects have been done for pure metals, or metals containing small amounts of impurities. The reason is that for fully quantitative studies, an accurate interatomic potential is necessary. In this study, the interest is in intermetallic compounds, which are concentrated alloys. Since this study will not approach the more difficult subject of obtaining accurate potentials for

alloys, the focus will be on qualitative and semi-quantitative results.

III. COMPUTER SIMULATION AND MODEL DEVELOPMENT

A. THE COMPUTER MODEL AND RELATED PROGRAMS

1. BCT

The computer simulation used in this study is called BCT, which is a program developed by the late Professor D. E. Harrison of the Naval Postgraduate School. This program used multiple-interaction (MI) timestep logic, since many events occur simultaneously. The program BCT allows the simultaneous computation of the position and velocity of an atomic particle, which are obtained via a numerical solution to Newton's laws of classical mechanics [Ref. 25].

The initial input data to the program vary slightly, depending on the topic of study. For vacancy relaxation studies, the initial input data include the target crystalline structure, atomic masses, elements to be included in the crystal, and the locations of the vacancies. For the spontaneous-recombination studies, additional input includes the initial energy provided to one atom of the dumbbell interstitial, as well as the relative position of the interstitial in the crystal lattice. The atom which receives the momentum impulse may travel in any direction in the lattice. The momentum is input using two angles, theta and phi, which are the direction angles in a spherical coordinate system. In the code, theta is the angle between the momentum

vector and the positive y-direction, and phi is the angle between the positive x-direction and the projection of the momentum on the surface plane. The geometry is indicated in Figure B1.

The computer program also has the capability of including inelastic energy loss. In all studies, the input variable ICVIN will determine whether or not inelastic losses due to electronic effects are to be included. The Lindhard Inelastic Loss Model [Ref. 26] is used to simulate electronic energy losses, which arise due to interactions between moving charges and free electrons in the lattice. The losses are represented in terms of the electronic stopping power, S_e, which is defined as:

$$S_e = 8\pi h a_b (Z_1)^{7/6} (Z_2/Z_{eff}) \quad , \tag{1}$$

where a_b is the Bohr radius,

$$a_b = h^2/4\pi^2 me^2 \quad , \tag{2}$$

and,

e = the electronic charge

m = the electron mass

Z_1 = atomic number of a moving particle

Z_2 = atomic number of the lattice atom

h = Planck's constant

$$Z_{eff} = (Z_1^{2/3} + Z_2^{2/3})^{3/2} \quad . \tag{3}$$

The constant Z_{eff} is the effective charge of the two interacting atoms. For all studies, the value for S_e was $1.44*10^{-13}$ kg/s. The electronic stopping power is

essentially a friction force, and acts to dampen the forces that arise due to the interatomic potentials. The model assumes that the electronic stopping power is proportional to the velocity of the moving atom [Ref. 27]. In all further discussions, electronic energy losses will be referred to as EE losses.

The program develops the collision cascade while continuously tracking the positions and velocities of lattice atoms in time. If the positions and velocities were computed for all lattice atoms every timestep, excessive computer run time would be used. Therefore, forces are not computed on a lattice atom unless this atom is within 2.4 LU from a moving atom. The program maintains a list of neighbors to moving atoms, which is periodically updated. In addition, to save computer time, the timestep increment is variable, and is obtained by dividing a specified distance by the speed of the highest atomic velocity in the crystallite. The specified distance is 0.1 LU, with the lattice unit being defined as one-half the lattice parameter, a_o. The program is run for a specified number of timesteps, usually enough to establish a lattice in equilibrium, or to infer the approach to equilibrium.

2. Ancillary Programs

Several other subprograms are used in the simulation to support the main program. Several of the important programs are discussed below.

a. INTEG

This program performs all of the numerical integrations encoded in the simulation. Newton's laws of motion are used to calculate the positions and velocities of atoms in the lattice.

b. POTVEC

This program calculates the forces and potential energies for all moving atoms and their neighbors. Forces are obtained by interpolating force tables, and potential energies by integrating force tables.

c. POTIN and POTFN(K)

These programs involve the identification of input potential function parameters, and the creation of the potential tables. The forces on atoms in the crystallite are obtained from these tables.

d. BCT001

This program generates a body centered tetragonal (BCT) lattice, which is entirely equivalent to an FCC structure. The crystallite faces are $(100)_{FCC} = (010)_{BCT}$, $(011)_{FCC} = (001)_{BCT}$, and $(011)_{FCC} = (100)_{BCT}$.

e. HALLOY

This program generates an $L1_2$ crystal structure as indicated in Figure B2, when an ordered lattice is selected. When a disordered lattice is desired, Al atoms are inserted at random locations in the crystal, keeping the composition $Zr_{75}Al_{25}$.

B. PROPERTIES OF Zr AND Zr_3Al

A summary of various properties and physical constants for Zr and Zr3Al is shown in Table A4 which was obtained from several sources [Ref. 28-30].

Table A3 shows that there are two equilibrium crystalline structures for pure Zr, hexagonal close packed (HCP) below 860°C, and body centered cubic (BCC) above this temperature. The phase diagram for the Zr-Al binary system is shown in Figure B3. The beta phase corresponds to the HCP structure of Zr, and the alpha phase corresponds to the BCC structure. The figure also shows that Zr_3Al forms via a peritectoid reaction [Ref. 28],

$$Zr_2Al + Zr \rightarrow Zr_3Al \ .$$

A peritectoid reaction is one in which two solids combine to produce a third solid on cooling. The peritectoid equilibrium is shown to occur at about 975°C, with a corresponding value of about 9% Al by weight.

This study involves the use of the program BCT001 which generates a body centered tetragonal crystal equivalent to the FCC structure which corresponds to Zr_3Al. This is evident in Figure B4, which contains the trigonometric relationships between the FCC lattice and the BCT lattice.

C. POTENTIAL FUNCTIONS

1. Basics

Multiple Interaction computer simulations involve the computations of forces between atoms. The forces are

obtained from a potential table, which in turn is formed by evaluating a chosen potential function. Therefore, if realistic data are desired, one must have an accurate potential function for the system being studied. Unfortunately, the exact form of interatomic potential functions and forces between two atoms are not known. The reason is that the problem is a complex, many-bodied problem, in that there are interactions between electrons with their respective nuclei, between electrons of one atom, and between electrons of both atoms. The problem is resolved by making approximations and assumptions, which lead to the selection of one of the many theoretical and empirical interatomic potentials available. Many different types of potential functions have been utilized in radiation damage studies. The potential functions used in this study are discussed briefly below. More detailed descriptions of the potential functions can be found in Torrens [Ref. 31].

a. Moliere

The Moliere potential function is a purely repulsive potential function. It is convenient to use this function to represent the wall of an interatomic potential. It is categorized as a "screened coulomb potential," and is an approximation to the Thomas-Fermi screening function [Ref. 31]. Basically, it is used for small interatomic distances, whereby the nuclei of the two atoms exert

coulombic forces on each other. The form of the screened interatomic potential is:

$$V(r) = (Z_1 Z_2 e^2/r) f(r). \quad (4)$$

The general form of the Moliere interatomic potential is:

$$V(r) = (Z_1 Z_2 e^2/r)(0.35\exp(-0.3r/a) + 0.55\exp(-1.2r/a) + 0.1\exp(-6.0r/a). \quad (5)$$

The variable "a" is the Firsov screening length, which is defined as:

$$a = k\ 0.855 a_b/(Z_1^{1/2} + Z_2^{1/2})^{-2/3} \quad (6)$$

and usually k=1, but here k will be an adjustable variable near 1 for providing a smooth spline, to the potential well.

b. MORSE

The Morse potential function is both an attractive and repulsive function, depending on the interatomic distance. This function is used in sputtering simulations and radiation damage studies as the attractive part of the interatomic potential function. It has the form:

$$V(r) = D_e \exp[-2a(r-R_e)] - 2D_e \exp[-a(r-R_e)]. \quad (7)$$

D_e is the depth of the potential well, R_e is the equilibrium interatomic separation distance, and a is usually the bulk modulus or the compressibility. However, Harrison [Ref. 32] finds it more beneficial to leave "a" as an adjustable parameter. The parameter "a" can then be used to match this attractive Morse potential to the repulsive Moliere potential at some separation.

c. Composite Morse-Moliere

In this study, the repulsive wall of the Moliere function is joined with one cubic spline to the attractive Morse function. First, the a term in the Morse and the k term of the Moliere are adjusted to allow a smooth match between the two functions, and then the cubic spline connects the two. In this way, there exists a potential function over a finite range of interatomic separation distances, and molecular dynamics studies of vacancies and interstitials can be conducted.

2. Selection of Potential Function Parameters

A composite Morse-Moliere interatomic potential function was used in this study. The potential function used in all simulation trials is indicated in Figure B5. The potential function used was the same, regardless of whether the code was run using pure Zr, or with the alloy. This will be discussed further below. The potential parameters chosen are indicated in Table A5. The terms a and k were selected in order to obtain a smooth potential function curve. The well depth value was chosen to match the cohesive energy for pure Zr, which is 6.316 eV. The equilibrium separation distance was set to 3.09 Å (the lattice parameter of Zr3Al is 4.372 Å). The values R_a and R_b are the spline boundaries. Between these values the spline matches the two curves. The value R_c is a cut-off distance beyond which potential and forces are zero.

IV. RESULTS

A. RELAXED ATOMIC CONFIGURATIONS

1. General

Various vacancy sites were used in order to study the relaxed atomic configurations around a vacancy or vacancy cluster. This study focuses on single vacancies, di-vacancies, and tri-vacancies. Various input parameters were changed in order to study their effects on the displacements of atoms surrounding the vacancy or cluster of vacancies. For example, simulations were performed with and without friction forces, and with an alloy or pure Zr.

In each trial performed, the displacements of atoms surrounding the vacancy or vacancies were computed. Average atomic displacements were computed for first nearest neighbors and second nearest neighbors. Nearest neighbors are lattice atoms separated by 1.414 LU, and second nearest neighbors are separated by 2 LU. In each tri-vacancy run, the nearest neighbors of one vacancy were identified so as to track the distance of each neighbor atom to the vacancy each timestep. Plots were made of this separation distance versus the elapsed time. This was done in order to visualize the effects of various parameters on the oscillatory motion of the lattice atoms.

2. Single Vacancy Results

One configuration was used to study the atomic displacements caused by a single vacancy. The atom which was removed from the lattice to create a vacancy was the body centered atom of the BCT unit cell. This configuration is portrayed in Figure B6. Two trials were performed, as indicated in Table A6. Trials 1 and 2 were performed with no EE losses. Trial 1 was performed with a Zr lattice, and trial 2 was performed with an alloy.

The quantity of interest in these two trials was the effect of the crystal type on the average atomic displacements, which are produced when the lattice relaxes to a new stable configuration. Specifically, the difference in mass, or the "mass effect," between the two runs, was of interest. Since the interaction potential between the Zr and Al atoms are the same, the static configuration of the alloy should be the same as that of the pure metal. However, in inducing the motion of atoms by the creation of a vacancy, then the differing mass of the two particles will affect their dynamics. This could possibly have the effect of producing different configurations for the relaxed crystal, both of which correspond to local minima in the potential energy.

The spatial arrangement of atoms about the single vacancy is portrayed in Figure B6. The body centered position has 12 nearest neighbors, and 6 second nearest

neighbors. As shown in Figure B6, there are two classes of first nearest neighbors, which are marked F1 or F2. The class F1 corresponds to first nearest neighbors which occupy body centered positions in cells adjacent to the one containing the vacancy. There are 4 class F1 first nearest neighbors. The class F2 corresponds to the 8 atoms which lie on the corners of the BCT unit cell containing the vacancy. There are 6 second nearest neighbors comprising class S1. The reason for this classification scheme is because it is found that the neighbors in these sites have different relaxed configurations whose final displacements are approximately the same.

The average atomic displacements for class F1, F2, and S1 are contained in Table A6. For Zr, or Trial 1, the first nearest neighbors comprising class F1 show the largest average atomic displacement, -0.0159 LU, which is inward, or towards the vacancy, as indicated by the minus sign. The first nearest neighbors comprising class F2 show an inward displacement of -0.0074 LU. Thus, a first nearest neighbor occupying a body centered position, adjacent to a cell containing a vacancy in a body centered position, has the larger displacement. The second nearest neighbors, class S1, show an outward average displacement of +0.0065 LU. These results are in qualitative agreement with the results of copper [Ref. 22]. For trial 2, performed with an alloy, the average atomic displacements are, in general, smaller than

for Zr. However in both cases the atoms in the relaxed configurations had lower potential energies than before relaxation. For example, in both the alloy and Zr lattice, the value for the initial potential energy of S2 atoms was -5.73 eV. Typical values for the potential energy after relaxation were -5.81 to -5.91 eV for the alloy, and from -5.42 to -5.71 eV for Zr.

3. Di-Vacancy Results

Two distinct configurations were used to study the atomic displacements caused by a di-vacancy. The vacancies were located at sites marked with open symbols in Figures B7 and B8. Figures B7 and B8 correspond to configurations D1 and D2, respectively. Six trials were performed, three on each configuration. In two of the trials, the run was performed with EE losses, but with either an alloy or pure Zr. This was done to determine if there was a noticeable effect of the mass difference under conditions of EE losses. Also, for each configuration, two trials with pure Zr, one with and one without EE losses, were compared. This was done to see if there was an effect of EE losses on the final atomic displacements.

The initial input parameters and average atomic displacements for di-vacancy configuration D1 are contained in Table A7. In this configuration, there were five classes of nearest neighbors, F1, F2, F3, S1 and S2. Examples of the spatial arrangement of four of these classes are contained in

Figure B7. The atoms labelled F1 in Figure B7 correspond to first nearest neighbors of one vacancy. These atoms lie in a body centered position of a unit cell adjacent to the vacancy, as shown in Figure B7. There are eight class F1 atoms. The atoms labelled F2 are first nearest neighbors to one vacancy, which lie in the corners of adjacent unit cells. There are eight class F2 atoms. Atoms labelled F3 are first nearest neighbors to both vacancies. These four atoms lie in the body centered plane located between the two vacancies. Atoms labelled S1 are second nearest neighbors, and lie in corners of adjacent unit cells. There are eight class S1 atoms. Finally, atoms listed as S2 in Table A7 are second nearest neighbors to each vacancy, which are found by moving 2 LU in the +y or -y direction from the position of each vacancy. There are two class S2 atoms.

Table A7 shows that for each trial run, the average atomic displacement obtained for each nearest neighbor class did not significantly differ. The average atomic displacements were dependent on the spatial location of the atom about the vacancy. For example, F1 atoms were the only class which showed an inward displacement, that is, towards the vacancy. The value obtained for the average atomic displacement was on the order of -0.016 LU. Class F2 atoms moved away from the vacancy, on the order of +0.006 LU. Class F3 atoms moved away from the vacancy, on the order of +0.002 LU. Class S1 atoms moved away from the vacancy, on

the order of +0.012 LU. Finally, class S2 atoms moved away from the vacancy, on the order of +0.004 LU.

The input parameters and average atomic displacements for di-vacancy configuration D2 are contained in Table A8. In this configuration, there were five classes of nearest neighbors, F1, F2, F3, S1 and S2. Examples of the spatial arrangement of these classes are contained in Figure B8. The atoms labelled F1 in Figure B8 correspond to the body centered, first nearest neighbors of one vacancy. There are twelve class F1 atoms. The atoms labelled F2 are first nearest neighbors to one vacancy, which lie in corners of adjacent unit cells. There are four class F2 atoms. Atoms labelled F3 are also first nearest neighbors to one vacancy, and are located by moving 1 LU in the +z or -z direction from each vacancy. There are two class F3 atoms. Atoms labelled S1 correspond to second nearest neighbors, and lie in corners of adjacent unit cells. There are four class S1 atoms. Finally, atoms labelled S2 lie in corners of unit cells, which are found by moving 2 LU in the +y or -y direction from each vacancy. There are four class S2 atoms.

Table A8 shows that for each trial run, the average atomic displacements obtained for each nearest neighbor class did not significantly differ. This was the same result obtained from configuration D1 trials. Again, the average atomic displacements were dependent on the spatial location of the atom about the vacancy. For configuration D2, the

body centered, first nearest neighbors comprising class F1 moved inward, on the order of -0.017 LU. All other neighbors moved outward, and class F2 atoms moved away from the vacancy as much as class F1 atoms moved towards it.

In general, for di-vacancy studies, atoms located in body centered positions of cells adjacent to the cell containing the vacancy show the largest displacements. In both configurations, the direction of the displacements was towards the vacancy. The results also did not show any significant effect of EE losses or mass on the average atomic displacements for each class of nearest neighbors.

4. Tri-Vacancy Results

Two distinct configurations were used to study the atomic displacements caused by a tri-vacancy. The vacancies were located at sites marked with open symbols and a label "v" in Figures B9 and B10. Figures B9 and B10 correspond to configurations T1 and T2, respectively. Eight trials were performed, four on each configuration. For each configuration, two trials were performed with Zr, one trial with EE losses and the other without. The other two trials were performed with the alloy, one case with EE losses, and the other without. In this way, for each tri-vacancy configuration, investigations were made for observing any effects of EE losses or mass on the average atomic displacements.

The input parameters and average atomic displacements for tri-vacancy configuration T1 are contained in Table A9. In this configuration, there were four classes of nearest neighbors that were considered, F1, F2, F3 and S1. Examples of the spatial arrangement of these classes are contained in Figure B9. The atoms labelled F1 in Figure B9 occupy body centered positions of the six unit cells adjacent to the cell containing the tri-vacancy. The six atoms of class F1 are all first nearest neighbors to either vacancy V_1 or V2. The atoms labelled F2 are first nearest neighbors to one of the corner vacancies. There are six class F2 atoms. Atoms labelled F3 are the eight nearest neighbors to the body centered vacancy alone. Finally, atoms labelled S1 are second nearest neighbors to one of the vacancies. There are eight class S1 atoms.

Table A9 shows that for most runs, the average atomic displacements obtained for each nearest neighbor class did not significantly differ. The average atomic displacement was dependent on the spatial location of the atom about the vacancy. The only trial which did not follow this trend was trial 3. In trials 1, 2 and 3, the largest average atomic displacements were directed inward, towards the vacancy. First nearest neighbors of class F2 and second nearest neighbors of class S1 show outward displacements, with a magnitude less than that for class F1.

The input parameters and average atomic displacements for tri-vacancy configuration T2 are contained in Table A10. In this configuration, three classes of nearest neighbors were considered, F1, F2 and S1. Examples of the spatial arrangement of these classes are contained in Figure B10. The atoms labelled F1 in Figure B10 occupy body centered positions of cells adjacent to vacancy V1 and vacancy V3. There are eight class F1 atoms. The atoms labelled F2 occupy body centered positions of cells adjacent to vacancy V2. There are four class F2 atoms. Thus, class F1 and class F2 atoms are first nearest neighbors to the corresponding vacancies. Finally, atoms labelled S1 are second nearest neighbors to either of the vacancies. There are 14 class S1 atoms.

Table A10 shows that the average atomic displacements obtained for each nearest neighbor class did not significantly differ. The one exception was trial 3, where the average atomic displacements were low. The reason for this discrepancy has not been determined. The average atomic displacement was dependent on the spatial location of the atom about the vacancy. Atoms of class F1 moved towards the vacancy, on the order of -0.012 LU. Atoms of class F2 also moved towards the vacancy, by about -0.005 LU. Second nearest neighbors of class S1 moved away from their respective vacancies, by about +0.0115 LU.

5. Atomic Oscillations

In order to illustrate the transition to equilibrium, plots such as those indicated in Figure B11 were obtained. This was done for each tri-vacancy run. A reference point, the body centered vacancy of the tri-vacancy defect, was selected. Several first nearest neighbors associated with this body centered vacancy were chosen, and the position of the atom from the reference point was plotted versus time. In this way, equilibrium could be seen by a dampening of the oscillations of the atom about its equilibrium position. This was readily apparent in trials performed with EE loss. For non-EE loss trials, the oscillations continued for a longer time until equilibrium was reached, as is expected. As an example of these plots, Figure B12 shows the plot of a class F2 first nearest neighbor, and its distance from the body centered vacancy of configuration T2. The data was obtained from a lattice of pure Zr and no EE losses. Figure B12 shows that equilibrium occurred at about 10 picoseconds. The large reduction in oscillation amplitude define the equilibrium point. Figure B13 shows the same atom tracked with EE losses incorporated. In this case, equilibrium occurred in about 3 picoseconds.

In addition to determining the point of equilibrium, plots as described above were generated to investigate if there was an effect of mass on the oscillatory motion of atoms about the vacancy. Tri-vacancy configuration T2

trials were compared. One trial was performed using an alloy, and one with Zr. For both cases, no EE losses were used. Three atoms, which corresponded to geometrically distinct lattice sites about the vacancy, were selected for observation. For the alloy, the corresponding Figures are B14, B15 and B16. For Zr, the corresponding Figures are B17, B18 and B19. The periods of the atomic oscillations about the equilibrium position are contained in Table A11. The periods do not significantly differ, and are between 0.17 and 0.2 picoseconds. These are of the same order of magnitude as typical phonon frequencies although none have been explicitly determined for Zr.

B. RECOMBINATION STUDIES

1. Lattice Orientations and Terminology

Two lattice orientations were used in order to study vacancy-interstitial spontaneous recombination. The first orientation is indicated in Figure B20, and will be referred to as case 1. The second orientation is shown in Figure B21, and will be referred to as case 2. For both cases, the dumbbell consisting of the interstitial pair is centered about the body centered position of the BCT unit cell, with its axis parallel to the y-direction. The separation distance between the two atoms of the dumbbell was 0.7LU. The difference between the two cases was in the placement of the vacancy.

For case 1 trials, the vacancy was located in a corner of the BCT unit cell, which is a nearest neighbor position to the body centered position. For case 2 trials, the vacancy was located in the body centered position of a cell adjacent to that of the dumbbell, as indicated in Figure B21. In order to be consistent in discussing the atoms of the dumbbell, the one with the largest y-coordinate is referred to as the lead atom, which is marked with an "L" in Figures B20 and B21.

In order to visualize the results, two types of graphics were used. Three dimensional plots containing the initial and final positions of the vacancy's neighbor atoms were constructed. An example is shown in Figure B22. The initial positions are solid circles, and the final positions are marked with arrowheads. Vacancies are indicated with open circles or squares. When necessary for discussion, Al atoms for alloy trials are appropriately indicated. The other graphics output used was a plot of the separation distance versus elapsed time. The separation distance is defined as the distance between the lead atom of the dumbbell and the initial position of the vacancy.

2. Trial Description

In short, the lead atom of the dumbbell is given an energy impulse of a specific magnitude. The values of theta and phi allow the lead atom to follow any desired direction. Trials are performed for a lattice consisting of the Zr_3Al

alloy or pure Zr, with and without friction forces. A vacancy is positioned in one of two positions, corresponding to case 1 and case 2 trials.

A summary of the trials performed along with the initial conditions is listed in Table A12. The column headed momentum direction was obtained from selecting various theta and phi values. For example, a value of 0 for both theta and phi implies the momentum was in the +y-direction.

3. Recombination Results

Table A13 contains a list of the trials performed as well as the elapsed time to equilibrium, and the approximate separation distance at equilibrium. In recombination studies, equilibrium is defined as the time for the separation distance to be 0.15 LU or less, with small oscillations about this position. The value chosen is arbitrary, and serves as a basis for comparisons between various trials.

Trials performed under conditions in which only one input variable differed were compared. The results are described below.

a. Momentum Direction

In order to determine the effect of the initial momentum direction on recombination, comparisons were made on trials with the same initial configuration. The only variable in the runs was the momentum direction. For example, case 1 EE loss runs performed with an energy impulse

of 0.1 eV were compared. These correspond to trials 2,4,6 and 26. In all cases, the time required for equilibrium was 2.3 picoseconds, and the separation distance was 0.11 LU. Figure B23 shows the initial and final positions of the dumbbell and neighbors for trial 2, and comparisons of the positions for trials 4,6 and 26 did not significantly differ.

Similar comparisons were made for case 1 trials 10,12 and 14. In this case, the time required for equilibrium was 2.3 picoseconds, and the separation distance between the vacancy and interstitial was 0.11 LU. Figure B24 shows the initial and final positions of the dumbbell and neighbors for trial 14, and comparisons of the positions for trials 10 and 12 did not significantly differ.

Thus, it appears that for the given trial configuration, the final position of the lead atom is independent of its initial direction, and hence its inertia. The simulations were terminated after 1200 timesteps, usually around 5 picoseconds. Recombination occurred to the extent that there was always some small separation between one atom of the dumbbell and the vacancy. However, relaxation towards equilibrium might either take many more timesteps or never occur. This is an intrinsic aspect of the molecular dynamics approach since a large set of atoms have been set in motion and need to disperse the initial imported kinetic energy. "Perfect" recombination between the vacancy and dumbbell cannot be seen during the timescale of the simulation. In

all trials performed, the second atom of the dumbbell repositioned itself to the body centered position of the BCT unit cell.

b. Orientation

In order to determine the effect of defect orientation on recombination, comparisons were made between case 1 and case 2 trials.

Trials 1 and 20 were non-EE loss trials. Figure B25 shows the initial and final positions of trial 1 at time 2.94 picoseconds, and Figure B26 shows the same for trial 20 at time 3.27 picoseconds. Both "snapshots" of the lattice were taken at approximately equal times. The most noticeable difference between the two is that the recombination is in a more advanced state for trial 20. From Figure B25, recombination is still occurring. The separation distance between the lead atom in the dumbbell and the vacancy is 0.25 LU. Figure B25 also shows much motion for neighboring atoms. Thus, there seems to be a preferred orientation for recombination, that being the dumbbell as oriented as in case 2.

Trials 2 and 21 were trials conducted with EE loss incorporated in the simulation. Figure B21 shows the initial and final positions of trial 2 at time 3.92 picoseconds, and Figure B27 shows the lattice for trial 21, at time 4.34 picoseconds. Again, recombination occurs quicker for trial 21. For trial 21, equilibrium occurs at

time 0.80 picoseconds, after which there are small oscillations of the lead atom about the position of the vacancy. For the case 1 trial, equilibrium occurred at 2.3 picoseconds, with a separation distance of 0.11 LU.

Trials 5 and 23 were non-EE loss trials. Figure B28 shows the initial and final positions of trial 5 at time 3.47 picoseconds, and Figure B29 shows the same for trial 23, at time 2.92 picoseconds. Again, it can be seen that the preferred orientation for recombination is a case 2 position. Equilibrium for trial 23 occurred at 0.9 picoseconds, with a separation distance of 0.07 LU. The separation distance for trial 5 was 0.21 LU.

c. Electronic Energy Losses

In order to determine the effect of EE losses on recombination, comparisons were made between trials using the same lattice orientation, energy, and momentum direction. Several pairs of data sets were analyzed. The pairs below were selected because they were done with different orientations and energies. This was done to show that the general effects of EE loss on recombination were the same regardless of other input parameters.

Trials 17 and 18 were case 1 trials with the lead atom of the dumbbell possessing an energy impulse of 0.001 eV in the y-direction. Trial 17 is the non-EE loss case, and trial 18 the EE loss run. Recombination is more likely to occur in the EE loss run than in the non-EE loss run. For

the EE loss case, the equilibrium separation distance was 0.11 LU, which occurred at time 2.3 picoseconds. In the non-EE loss case, the equilibrium separation distance was 0.22 LU. Figures B30 and B31 show the lattice positions for the non-EE loss and EE loss case, respectively. The lead atom of the dumbbell travels closer to the vacancy site in the friction case than the non-EE loss case. Also, the other dumbbell atom repositions to the body centered positions more evidently in the EE loss case. These effects probably arise due to the increased range of motion achieved in the absence of EE loss forces. Atoms will travel further and reach closer interatomic distances, and hence higher forces, in non-EE loss trials.

Trials 20 and 21 were case 2 trials with an energy impulse of 0.1 eV in the y-direction. In both cases, recombination occurred at 0.9 picoseconds, but in the EE loss case, the lead atom of the dumbbell is closer to the vacancy site by 0.04 LU in that time.

In general, trials performed with EE losses result in a more defined recombination within the time of the simulation. EE losses also reduce the oscillations of atoms about their equilibrium sites.

d. Alloy

In order to determine the effect of the mass of a lattice atom on recombination, various trials were performed using an alloy. Comparisons were made on trials which

differed only in the selection of either an alloy or pure Zr lattice. Several trials were chosen for discussion.

Trials 16 and 36 were case 1 trials with the lead atom of the dumbbell possessing an energy of 0.01 eV in the y-direction. For the alloy run, trial 16, the time to equilibrium was 0.5 picoseconds. For pure Zr, equilibrium occurred at 1.0 picoseconds. The separation distance for the alloy and pure Zr was 0.04 LU in each case. Figures B32 and B33 are illustrations of the atomic positions for the case of the alloy and Zr lattice, respectively. As seen from these plots, it does not appear the use of the alloy had an effect on the recombination process.

Trials 21 and 33 were case 2 trials with the lead atom of the dumbbell possessing an energy of 0.1 eV in the y-direction. As indicated in Table A10, equilibrium in both cases occurred at the same time and at the same separation distance. Figures B28 and B34 show the lattice positions, which support this observation.

In general, it seems that the use of an alloy or pure Zr does not significantly affect the recombination of the vacancy-interstitial defect.

V. CONCLUSIONS AND RECOMMENDATIONS

The results of this study show that the molecular dynamics approach is a valid tool which can be utilized in the study of atomic relaxation and vacancy-interstitial recombination.

Comparisons of the atomic relaxation studies show that the final average atomic displacements are not significantly affected by inelastic energy losses or the introduction of a mass effect. Rather, the atomic displacements are highly dependent on the initial orientation of the atom with respect to the vacancy. In general, atoms that are first nearest neighbors to a vacancy, and which occupy the body centered positions of cells adjacent to the vacancy, will move the most, and will move inward, towards the vacancy. Second nearest neighbors generally move away from the vacancy. These results are in qualitative agreement with static relaxation studies performed with single vacancies in FCC copper.

The studies performed on vacancy-interstitial recombination show that recombination is not affected by the inertia or the mass effect of the alloy. Electronic energy losses result in a more defined recombination during the timescale of the simulation. Also, there does seem to be a preferred orientation of the vacancy-interstitial defect, for

the two cases investigated. Recombination occurs faster with the vacancy oriented in a body centered position in a cell adjacent to the dumbbell. This is supported by the findings of the relaxation studies. The atoms which occupy the body centered positions adjacent to a body centered vacancy move the most. Since the dumbbell is oriented about the body centered position of a unit cell, and has a large potential energy due to the small interatomic distance, 0.7 LU, it is expected that the atoms of the dumbbell will move quickly to minimize the energy of the system.

Given that the atomic displacements obtained in vacancy relaxation studies are symmetrical, and correspond qualitatively with others results, this molecular dynamics technique should be used to study defect configurations. The code could be used for computing the average atomic displacements for lattices containing multiple vacancies. Also, the distance between the vacancy and the dumbbell could be manipulated in order to establish the distance beyond which recombination does not occur.

APPENDIX A - TABLES

TABLE A1. ORDERED INTERMETALLIC COMPOUNDS

Intermetallic Compounds	Crystal Structure
NiAl	B2
Ni_3Al	$L1_2$
$NiAl_3$	DO_{20}
CoTi	B2
Co_2Ti	C15
Cr_2Ti	C15
CuTi	B11
FeTi	B2
NiTi	B2
$NiTi_2$	$E9_3$
Ni_3Ti	DO_{24}
NbNi	$D8_5$
Zr_2Al	C16
Zr_3Al	$L1_2$
U_6Fe	$D2_c$

TABLE A2. DISPLACEMENTS OF ATOMS IN SHELLS AROUND A SINGLE VACANCY IN FCC COPPER.

Shell						
First	Second	Third	Fourth	Fifth	Sixth	Seventh
-0.019	+0.002	-0.003	-0.005	0	-0.002	-0.001

Note: Units are in terms of the lattice constant, which for copper is 3.603 Å.

TABLE A3. DISPLACEMENTS DUE TO A <100> DUMBBELL WITH A MODIFIED MORSE POTENTIAL

Shell	Displacement (a) s_x	s_y	s_z
dumbbell	0	0	0.3
011	0	0.08	0.04
110	-0.03	-0.03	0

Note: Displacements are in terms of the lattice constant for copper (3.603 Å).

TABLE A4. PHYSICAL DATA FOR Zr AND Zr_3Al

	Zr	Zr_3Al
Atomic Number (Z)	40	
Atomic Weight (amu)	91.22	
Density (g/cm^3)	7.253	5.976
Crystal Type	HCP, BCC	FCC (ordered)
Lattice Constant (A)	a_o=3.231 (HCP) c_o=5.144 (HCP) a_o=3.62 (BCC)	a_o=4.372
Valence	+2,+3,+4	

TABLE A5. POTENTIAL PARAMETERS

Well Depth (eV)	Equilibrium Separation Distance (Å)	Adjustable Parameters ($Å^{-1}$)		Spline Boundaries (LU)		Cut-off Distance (LU)
D_e	R_e	a	k	R_a	R_b	R_c
0.858	3.09	1.5	0.9	0.85	0.92	2.4

TABLE A6. AVERAGE ATOMIC DISPLACEMENTS FOR SINGLE VACANCY RELAXATION STUDIES

Trial	Crystal	EE Losses	Average Atomic Displacements for Various Nearest Neighbor Classes (LU) F1(4)	F2(8)	S1(6)
1	Zr	no	-.0159	-.0074	+.0065
2	Alloy	no	-.0004	+.0108	+.0026

TABLE A7. AVERAGE ATOMIC DISPLACEMENTS FOR DI-VACANCY RELAXATION STUDIES (CONFIGURATION D1)

Trial	Crystal	EE Losses	Average Atomic Displacements for Various Nearest Neighbor Classes (LU) F1(8)	F2(8)	F3(4)	S1(8)	S2(2)
1	Zr	no	-.0175	+.0075	+.0027	+.0124	+.004
2	Zr	yes	-.0150	+.0057	+.0020	+.0118	+.004
3	Alloy	yes	-.0150	+.0057	+.0023	+.0120	+.004

Note: The number in parentheses next to the nearest neighbor class represents the number of atoms in the class.

TABLE A8. AVERAGE ATOMIC DISPLACEMENTS FOR DI-VACANCY RELAXATION STUDIES (CONFIGURATION D2)

Trial	Crystal	EE Losses	Average Atomic Displacements for Various Nearest Neighbor Classes (LU) F1(12)	F2(4)	F3(2)	S1(4)	S2(4)
1	Zr	no	-.0170	+.0163	+.0061	+.0118	+.004
2	Zr	yes	-.0173	+.0166	+.0064	+.0074	+.004
3	Alloy	yes	-.0173	+.0167	+.0065	+.0094	+.004

Note: The number in parentheses next to the nearest neighbor class represents the number of atoms in the class.

TABLE A9. AVERAGE ATOMIC DISPLACEMENTS FOR TRI-VACANCY RELAXATION STUDIES (CONFIGURATION T1)

Trial	Crystal	EE Losses	Average Atomic Displacements for Various Nearest Neighbor Classes (LU) F1(6)	F2(6)	F3(8)	S1(8)
1	Zr	no	-.0252	+.0168	+.0070	+.023
2	Zr	yes	-.0152	+.0131	+.003	+.0134
3	Alloy	no	+.0046	+.0195	-.0140	-.0045
4	Alloy	yes	-.0152	+.0131	+.0030	+.0133

Note: The number in parentheses next to the nearest neighbor class represents the number of atoms in the class.

TABLE A10. AVERAGE ATOMIC DISPLACEMENTS FOR TRI-VACANCY RELAXATION STUDIES (CONFIGURATION T2)

Trial	Crystal	EE Losses	Average Atomic Displacements for Various Nearest Neighbor Classes (LU) F1(8)	F2(4)	S1(14)
1	Zr	no	-.0121	-.0003	+.0117
2	Zr	yes	-.0123	-.0006	+.0115
3	Alloy	no	-.0066	-.0012	+.0108
4	Alloy	yes	-.0121	-.0006	+.0112

Note: The number in parentheses next to the nearest neighbor class represents the number of atoms in the class.

TABLE A11. Oscillations

Atom	Period (picoseconds) Alloy	Zr
1	0.17	0.18
2	0.20	0.18
3	0.18	0.20

TABLE A12. INITIAL INPUT PARAMETERS FOR RECOMBINATION STUDIES

Trial	Crystal	Friction	Case	Energy (eV)	Momentum Direction Theta (°)	Phi
1	Alloy	no	1	0.1	0	0
2	Alloy	yes	1	0.1	0	0
3	Alloy	no	1	0.1	90	90
4	Alloy	yes	1	0.1	90	90
5	Alloy	no	1	0.1	45	45
6	Alloy*	yes	1	0.1	0	0
7	Alloy*	no	1	0.1	0	0
8	Alloy*	yes	1	0.1	0	0
9	Alloy	no	1	0.01	0	0
10	Alloy	yes	1	0.01	0	0
11	Alloy	no	1	0.01	90	90
12	Alloy	yes	1	0.01	90	90
13	Alloy	no	1	0.01	45	45
14	Alloy*	yes	1	0.01	45	45
15	Alloy*	no	1	0.01	0	0
16	Alloy*	yes	1	0.01	0	0
17	Alloy	no	1	0.001	0	0
18	Alloy	yes	1	0.001	0	0
19	Alloy	no	1	0.001	90	90
20	Alloy	no	2	0.1	0	0
21	Alloy	yes	2	0.1	0	0
22	Alloy	no	2	0.1	90	90
23	Alloy	no	2	0.1	45	45
24	Alloy	no	2	0.1	180	0
25	Alloy	no	2	0.1	90	180
26	Alloy	yes	1	0.1	180	0
27	Alloy	yes	2	0.001	90	270
28	Alloy	yes	2	0.01	0	0
29	Zr	yes	1	0.1	0	0
30	Zr	no	1	0.0001	0	0
31	Zr	yes	1	0.1	180	0
32	Zr	no	1	0.001	180	0
33	Zr	yes	2	0.1	0	0
34	Zr	yes	2	0.1	180	0
35	Zr	yes	1	0.001	0	0
36	Zr	yes	1	0.01	0	0

Note: * indicates a disordered alloy

TABLE A13. EQUILIBRIUM TIME AND SEPARATION DISTANCE FOR RECOMBINATION STUDIES

Trial	Time to Reach Equilibrium (picoseconds)	Equilibrium Separation Distance (LU)
1	N	-
2	2.3	0.11
3	N	-
4	2.3	0.11
5	N	-
6	2.3	0.11
7	3.2	0.12
8	0.5	0.13
9		
10	2.3	0.11
11	N	-
12	2.3	0.11
13	N	-
14	2.3	0.11
15	0.5	0.08
16	0.5	0.04
17	N	-
18	2.3	0.11
19	N	-
20	1.0	0.06
21	0.8	0.02
22	0.6	0.06
23	0.9	0.07
24	0.8	0.08
25	0.8	0.09
26	2.3	0.11
27	0.9	0.03
28	1.1	0.04
29	0.9	0.04
30	1.2	0.10
31	1.0	0.04
32	1.5	0.10
33	0.9	0.01
34	1.2	0.01
35	1.0	0.04
36	1.0	0.04

APPENDIX B - FIGURES

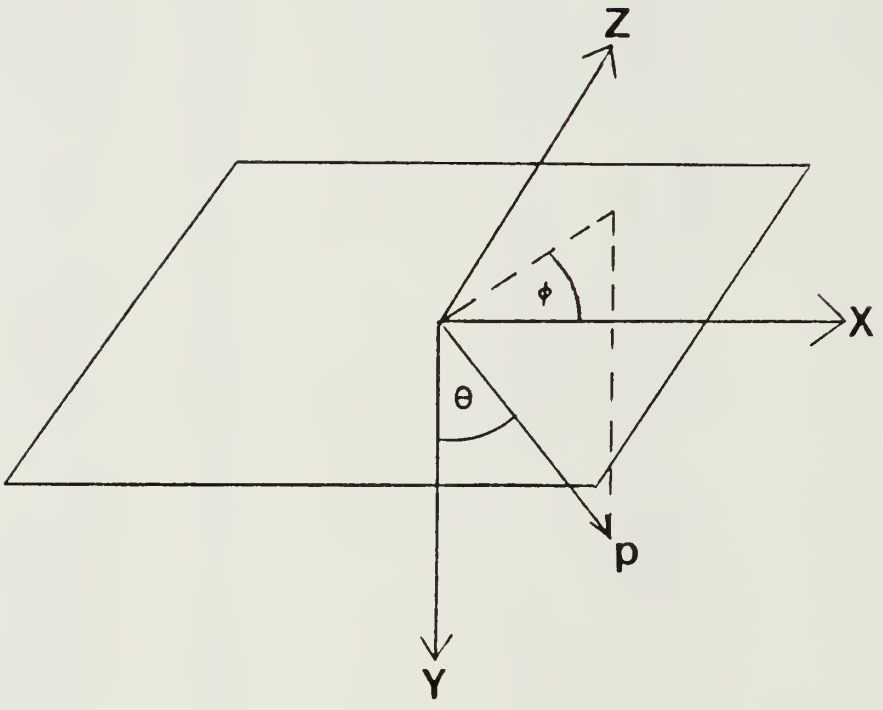

Figure B1. The Direction Angles Theta and Phi in Spherical Coordinates. The Plane is the Surface Normal of the Crystal. The Direction **y** is into the Crystal.

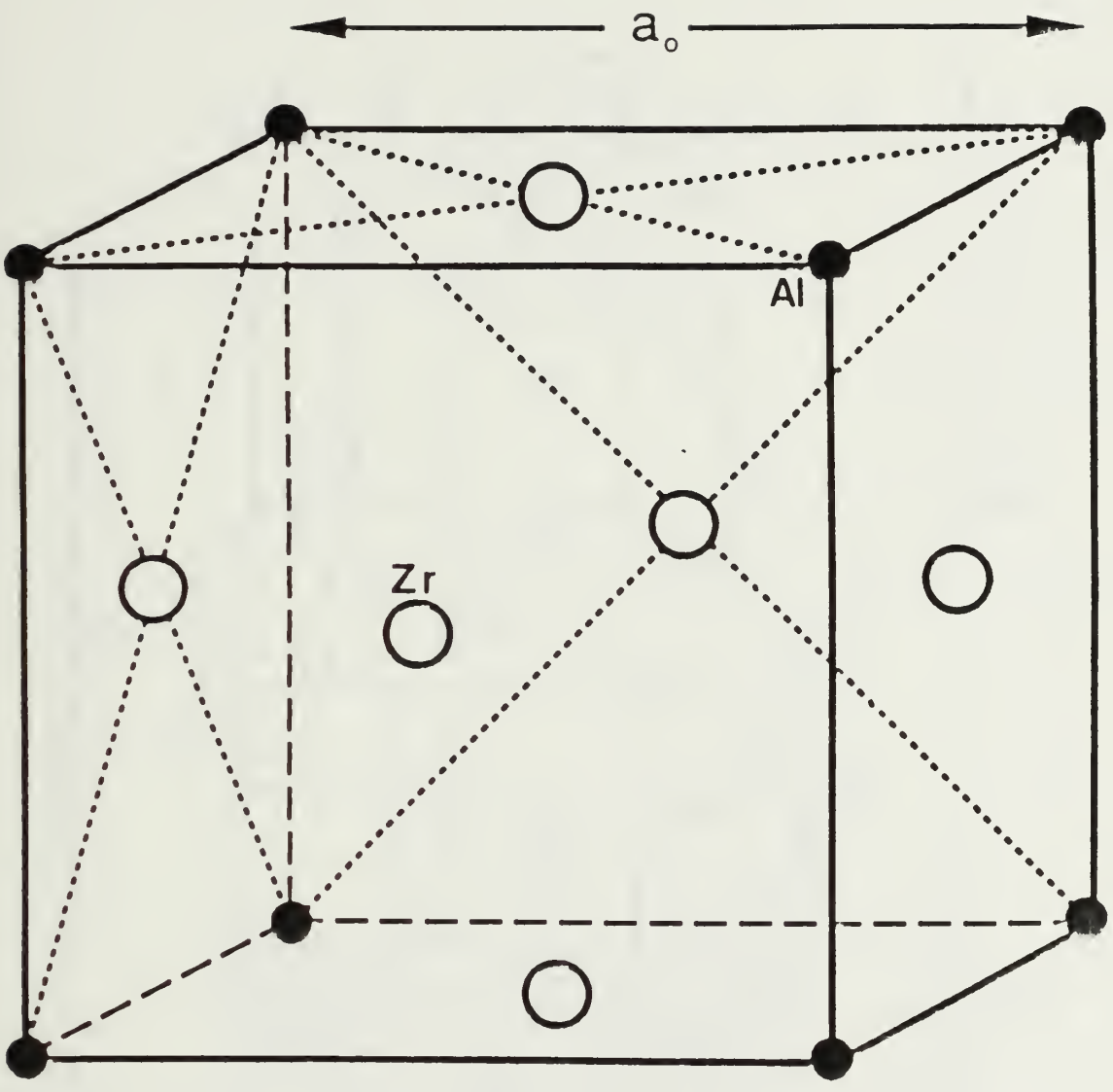

Figure B2. Illustration of a L12 (Ordered FCC) Lattice. The Length a_o is the Lattice Constant.

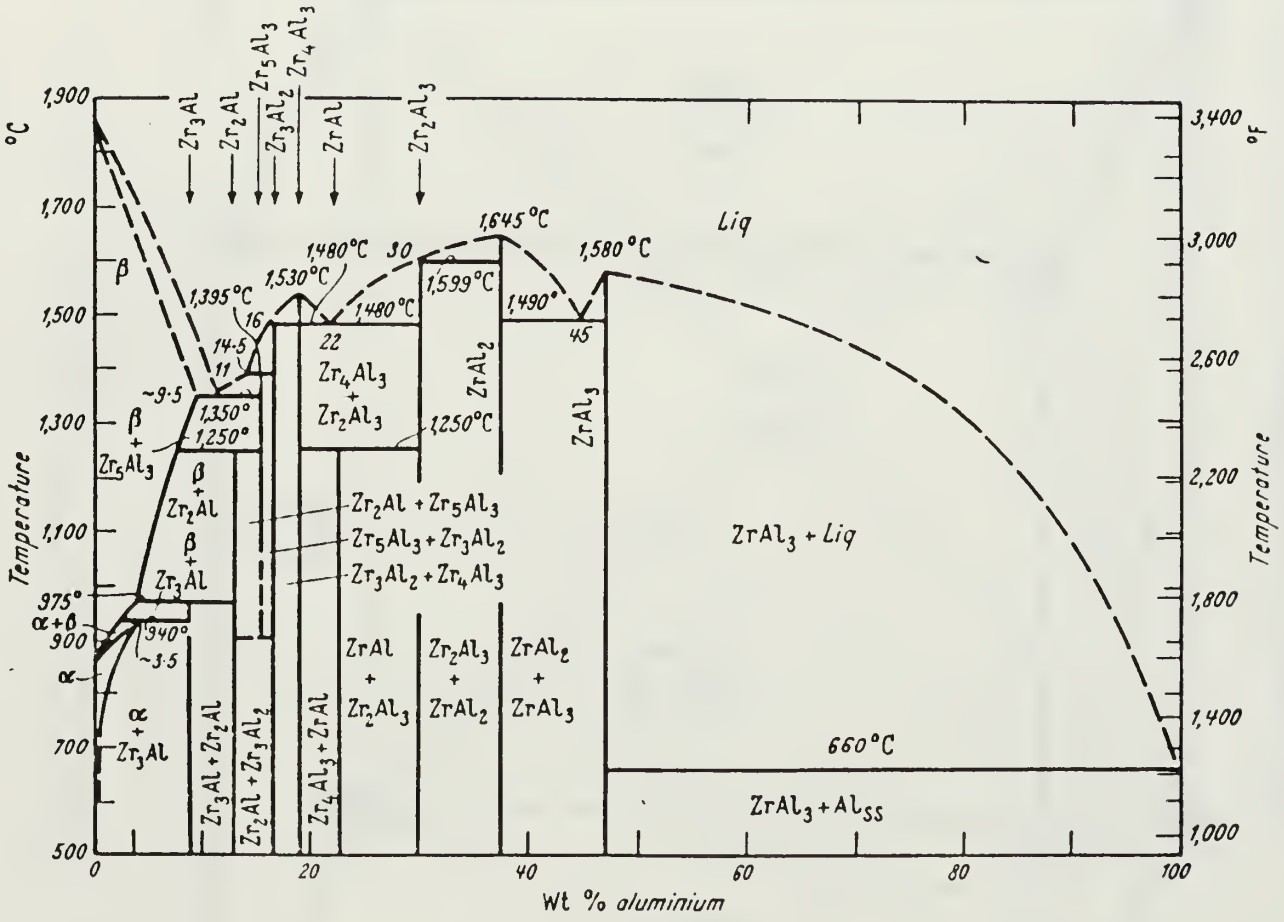

Figure B3. The Zirconium-Aluminum Phase Diagram.

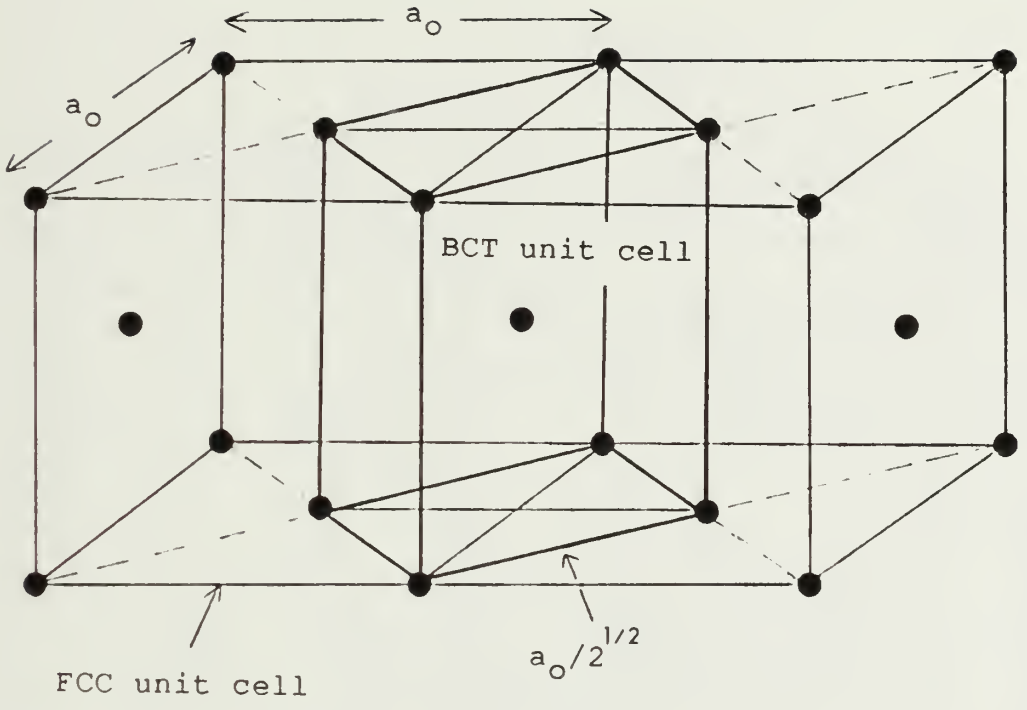

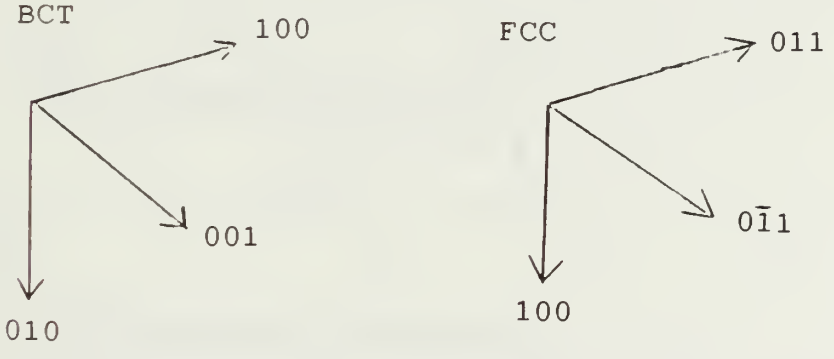

Figure B4. Trigonometric Relationships Between the FCC and BCT Crystal Lattice.

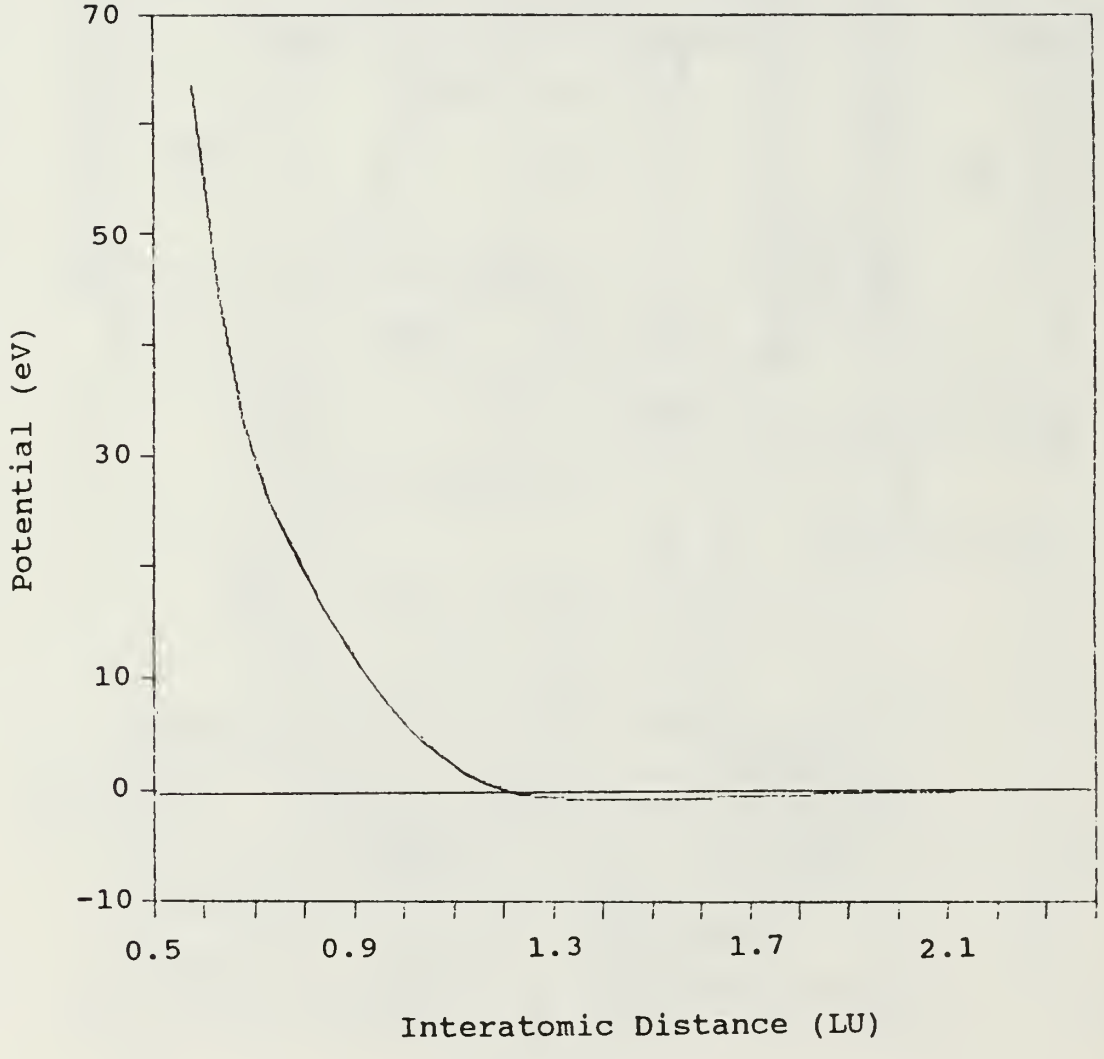

Figure B5. The Zirconium Potential Function.

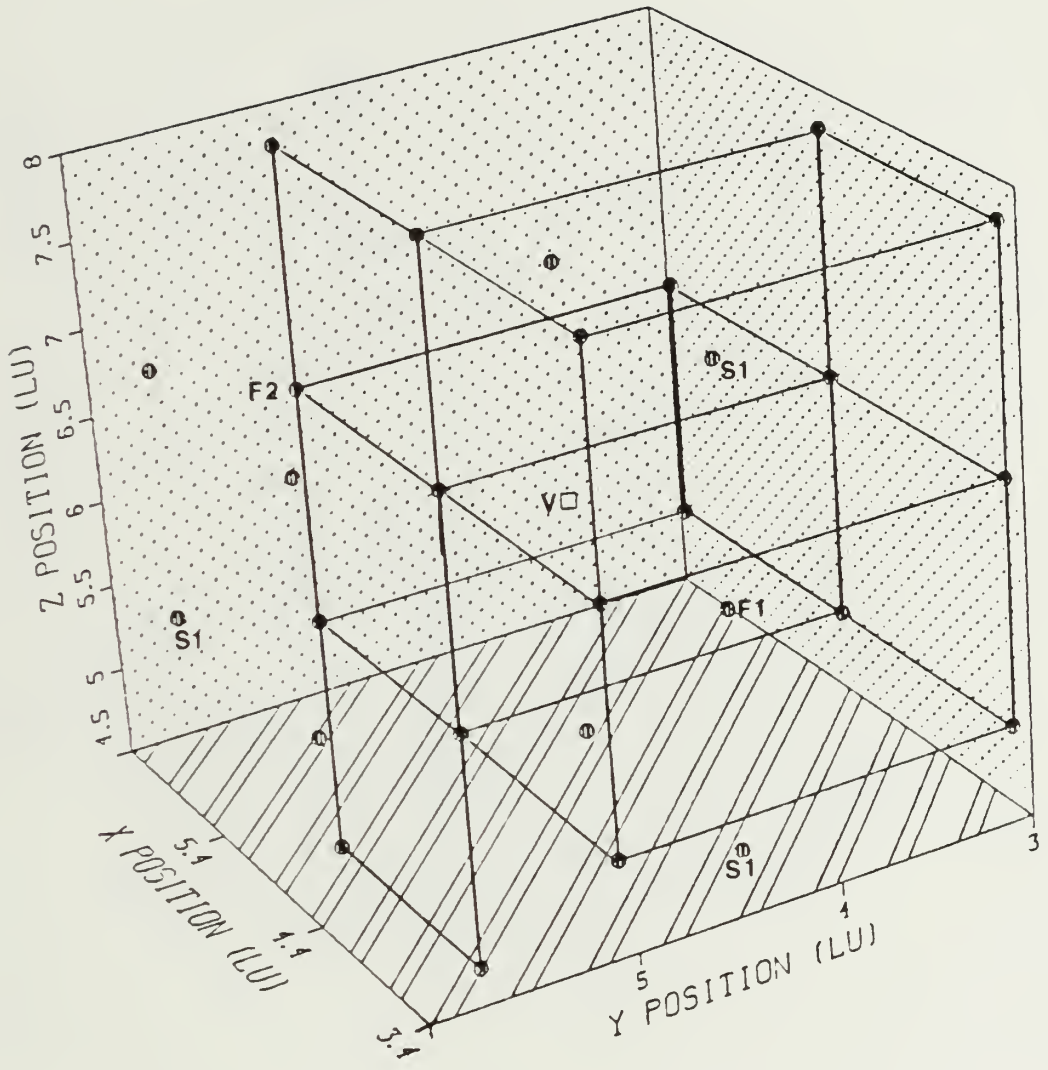

Figure B6. The Configuration for Single Vacancy Atomic Relaxation Studies. The Vacancy is Marked **v** and Examples of Atoms of Nearest Neighbor Class **F1**, **F2** and **S1** are Illustrated.

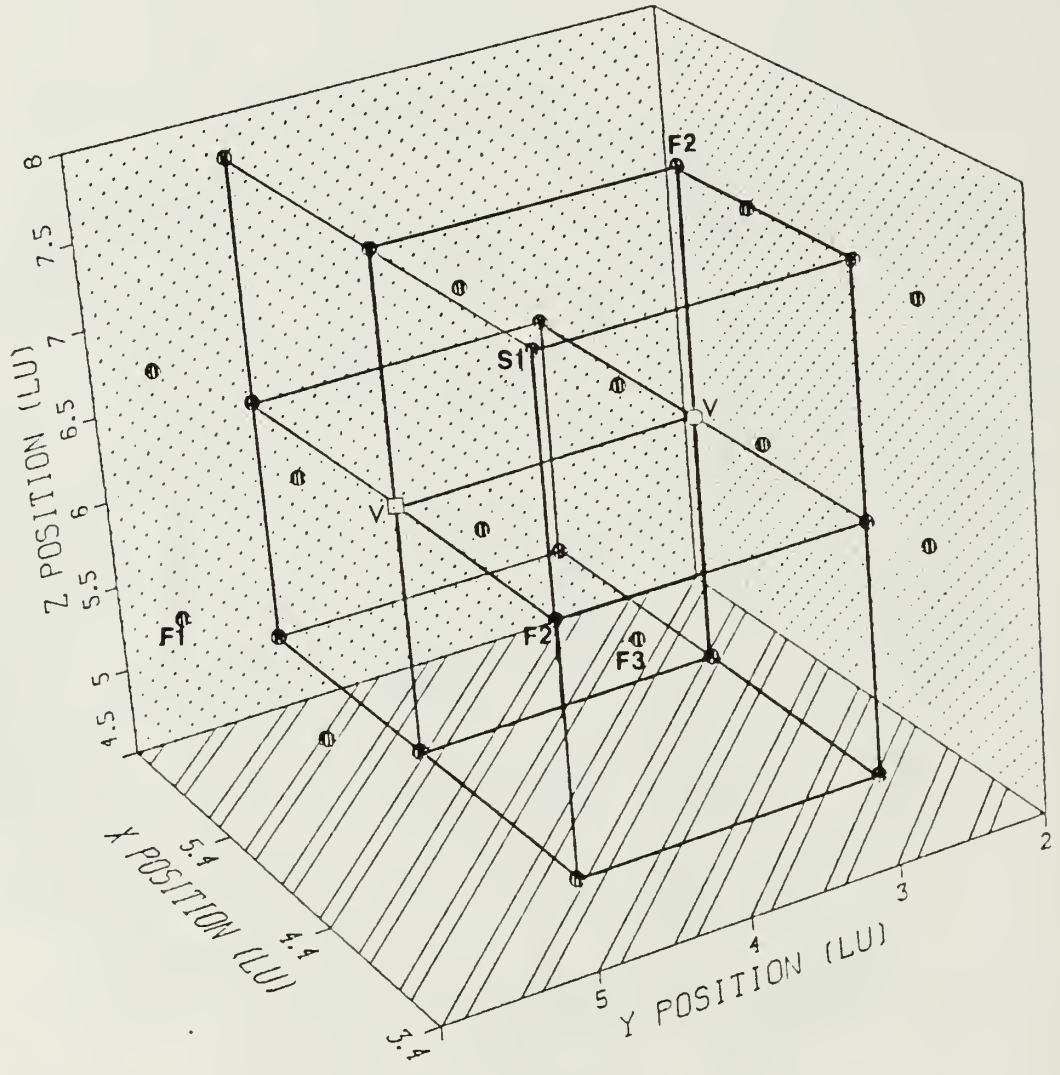

Figure B7. The Spatial Arrangement of Atoms for Di-Vacancy Configuration D1. The Two Vacancies are Marked **V** and Examples of Atoms of Nearest Neighbor Class **F1**, **F2**, **F3** and **S1** are Illustrated.

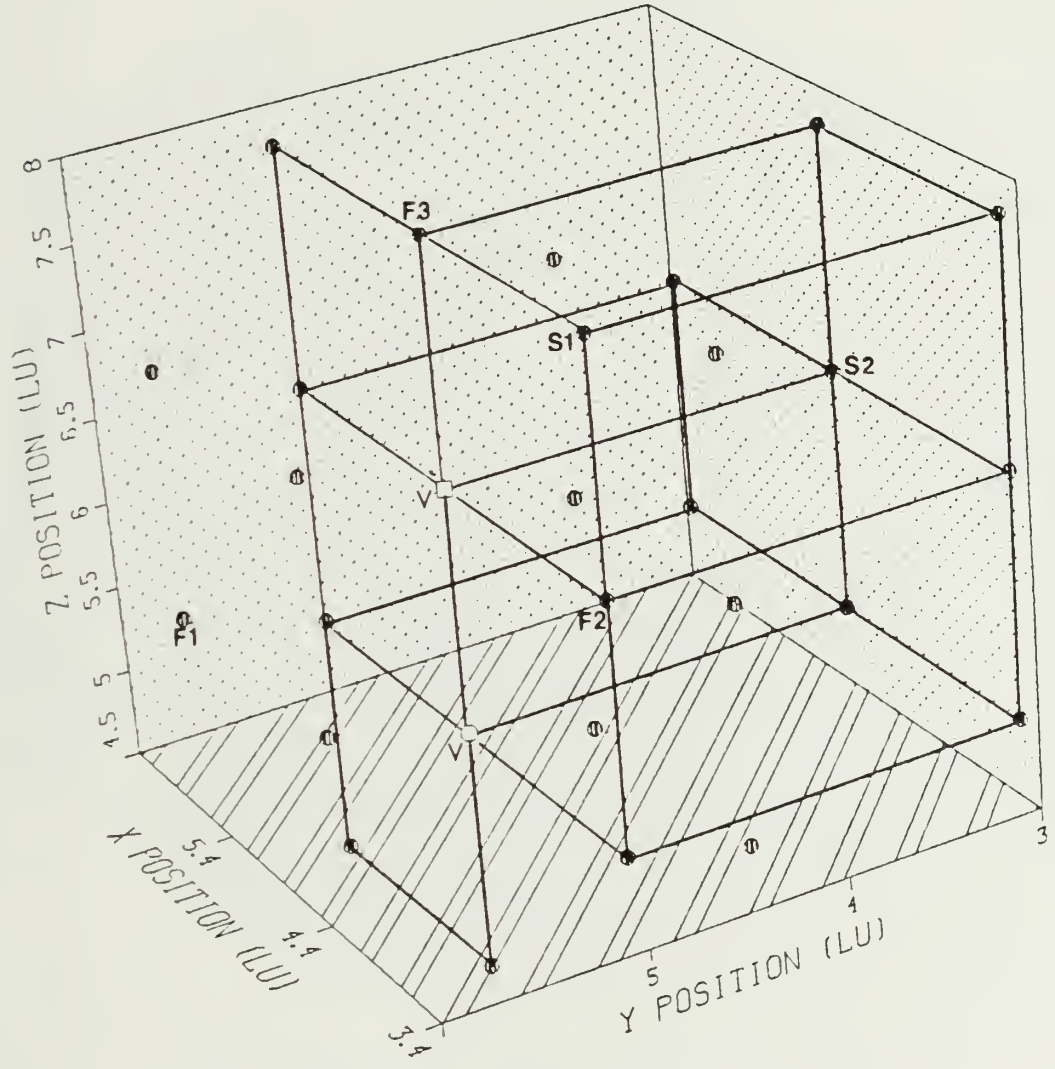

Figure B8. The Spatial Arrangement of Atoms for Di-Vacancy Configuration D2. The Two Vacancies are Marked **V** and Examples of Atoms of Nearest Neighbor Class **F1**, **F2**, **F3**, **S1** and **S2** are Illustrated.

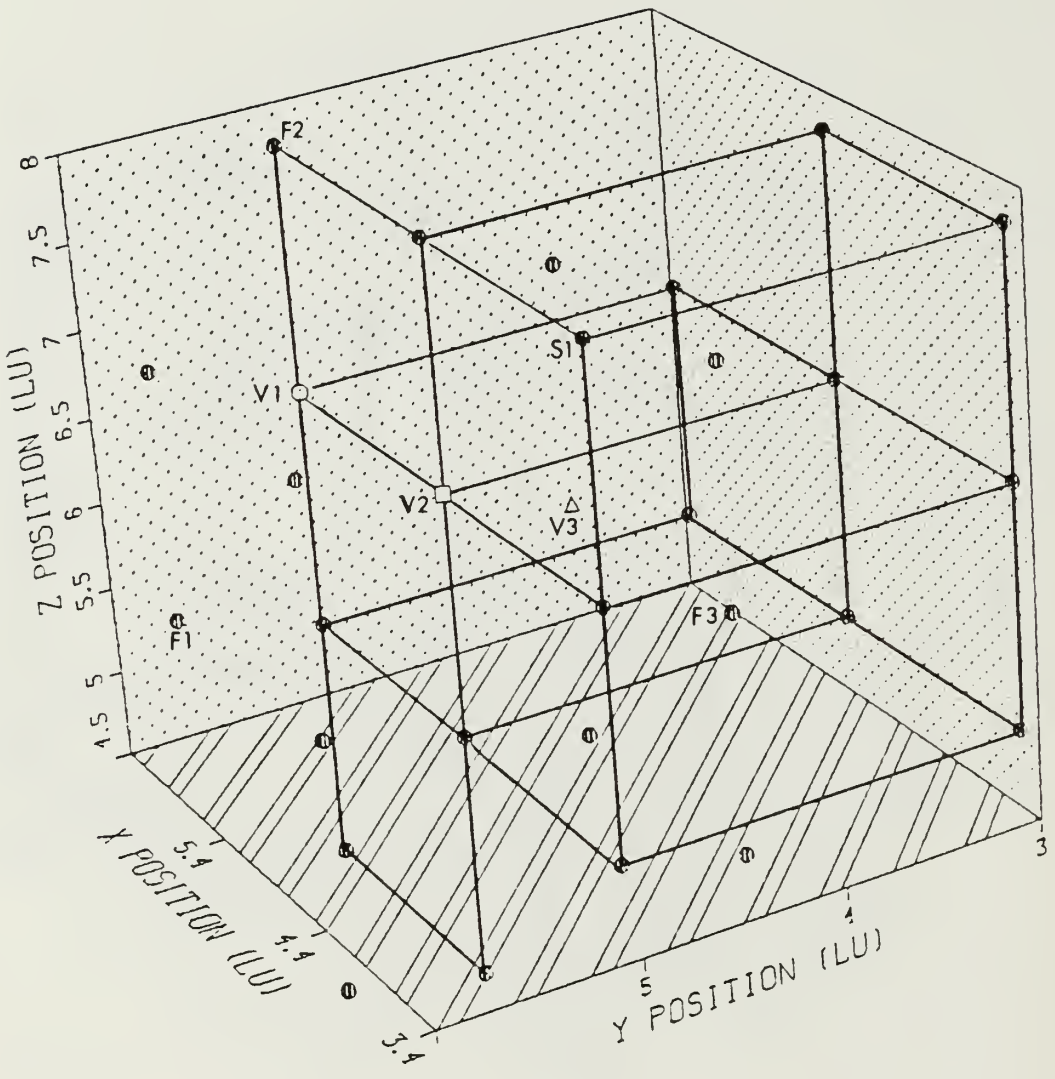

Figure B9. The Spatial Arrangement of Atoms for Tri-Vacancy Configuration T1. The Three Vacancies are Marked **V1**, **V2** and **V3**. Examples of Atoms of Nearest Neighbor Class **F1**, **F2**, **F3** and **S1** are Illustrated.

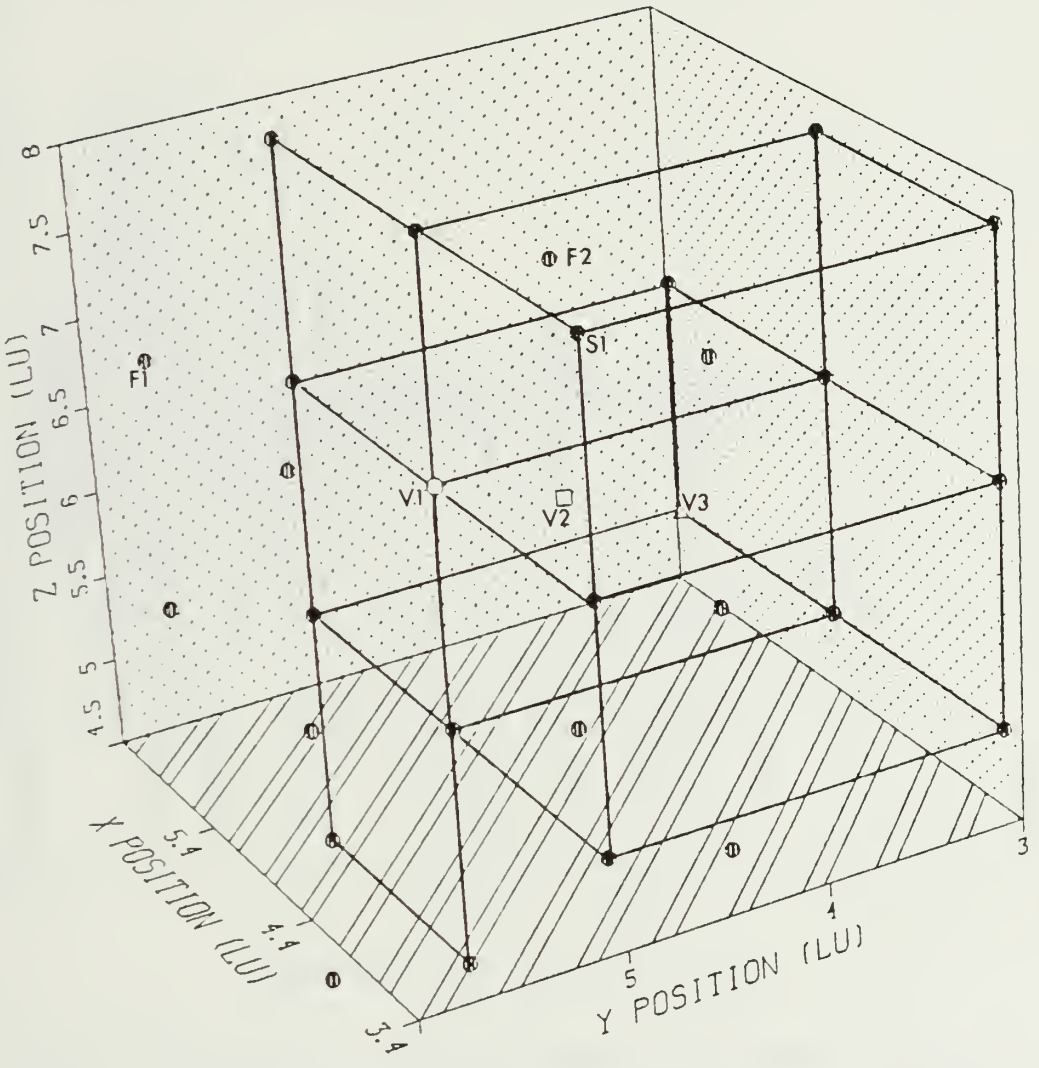

Figure B10. The Spatial Arrangement of Atoms for Tri-Vacancy Configuration T2. The Three Vacancies are Marked **V1**, **V2** and **V3**. Examples of Atoms of Nearest Neighbor Class **F1**, **F2** and **S1** are Illustrated.

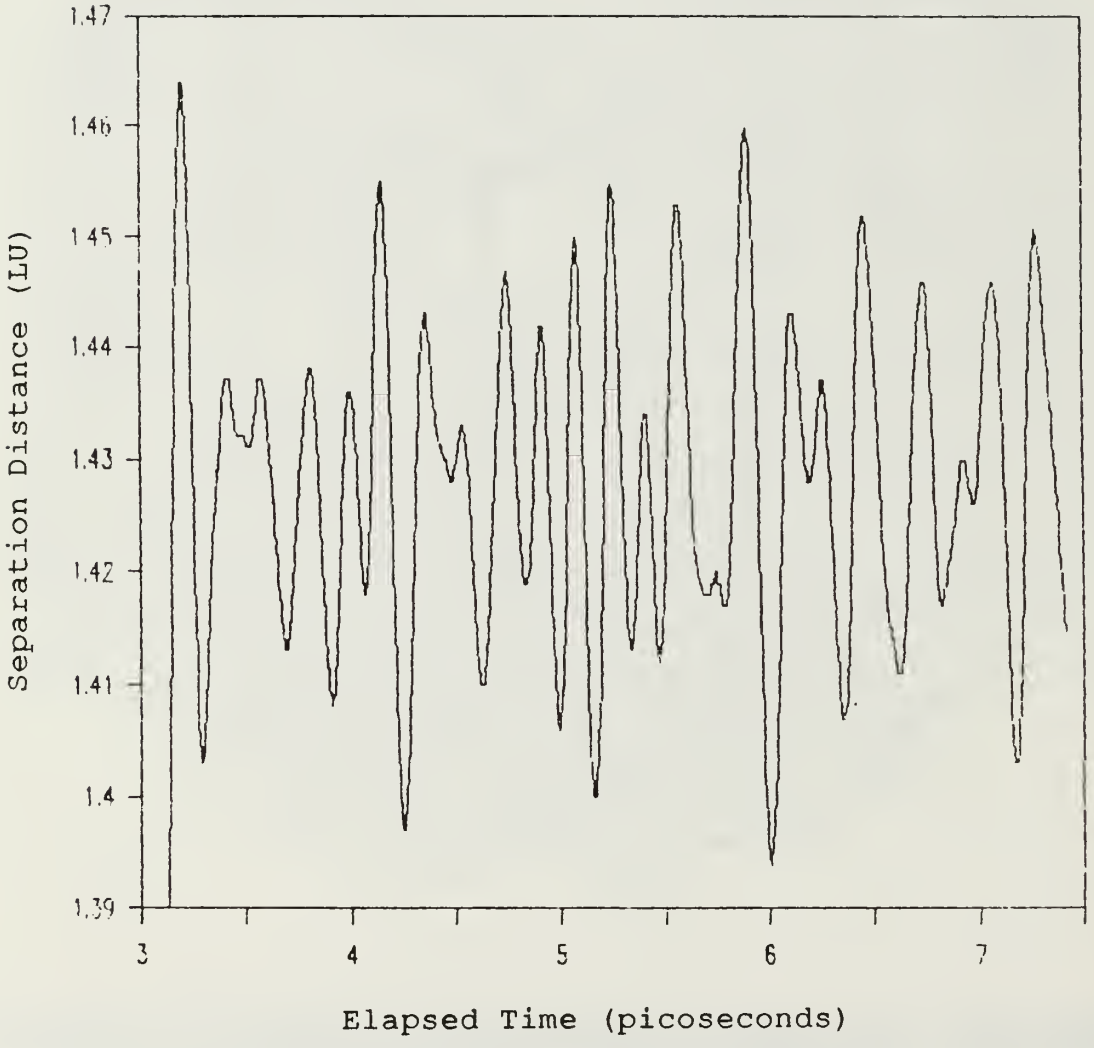

Figure B11. Sample Plot of the Separation Distance Between the Neighbor Atom and Body Centered Vacancy.

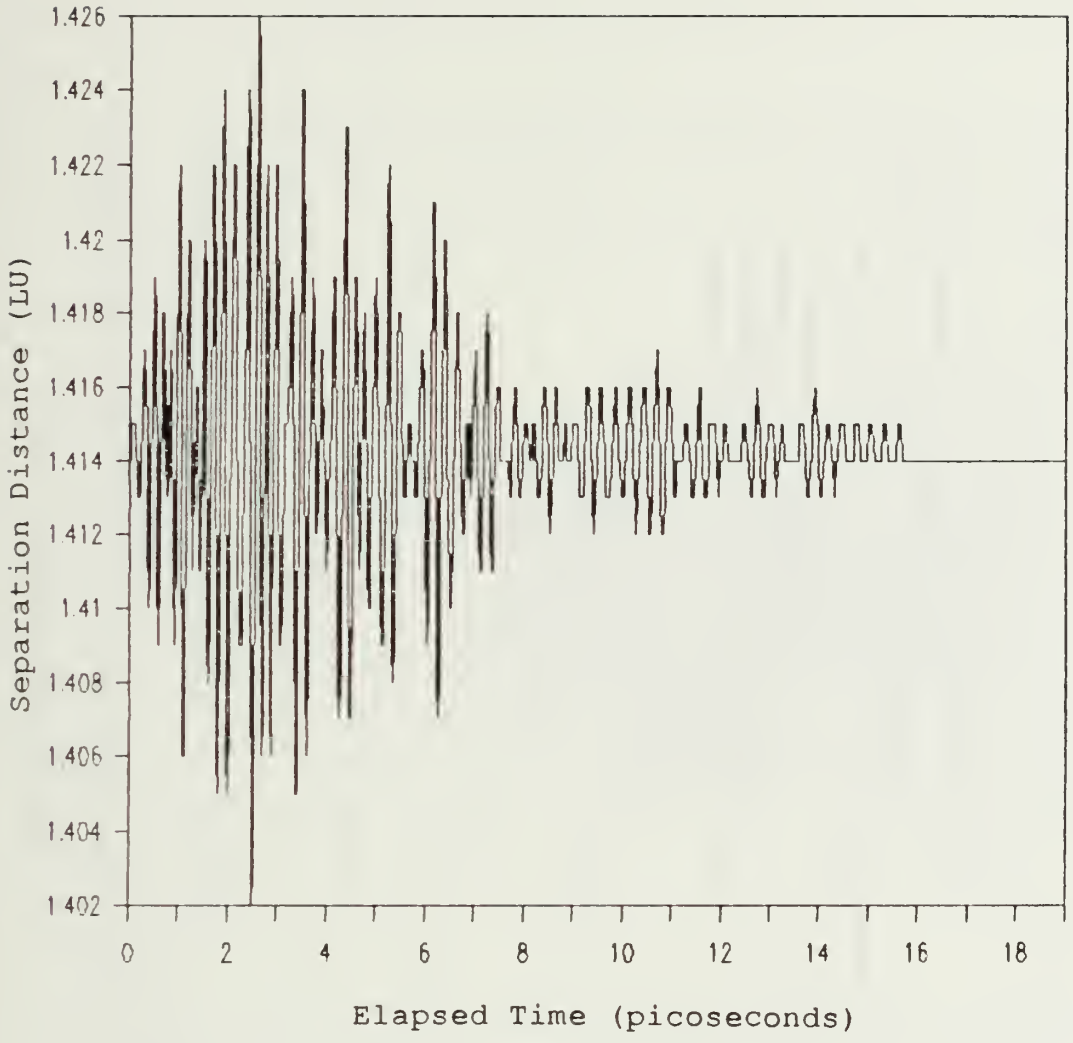

Figure B12. The Oscillation of a Class F2 Nearest Neighbor About the Body Centered Vacancy of Configuration T2. The Plot Was Obtained from a Lattice of Pure Zr Without EE Losses.

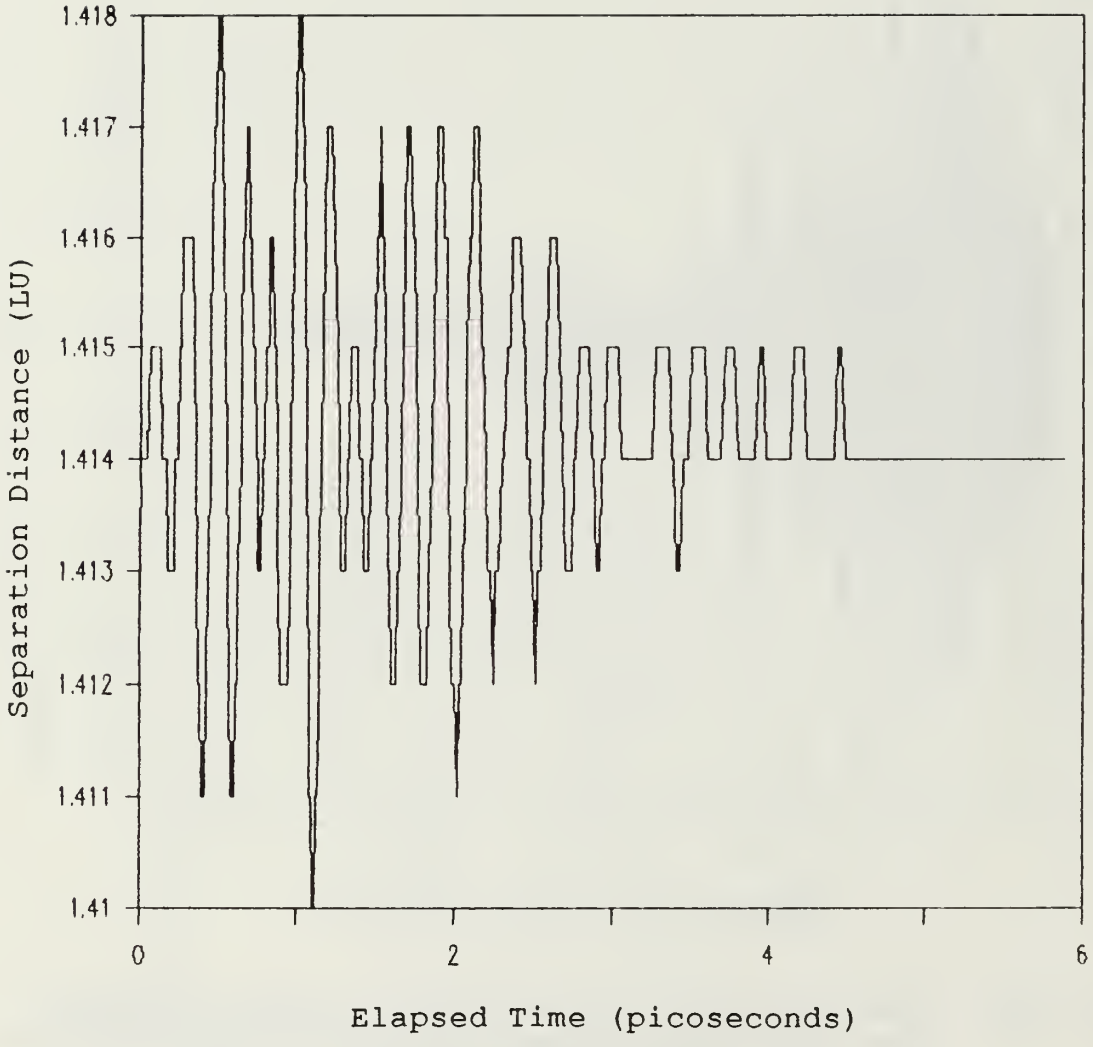

Figure B13. The Oscillation of a Class F2 Nearest Neighbor About the Body Centered Vacancy of Configuration T2. The Plot Was Obtained from a Lattice of Pure Zr With EE Losses.

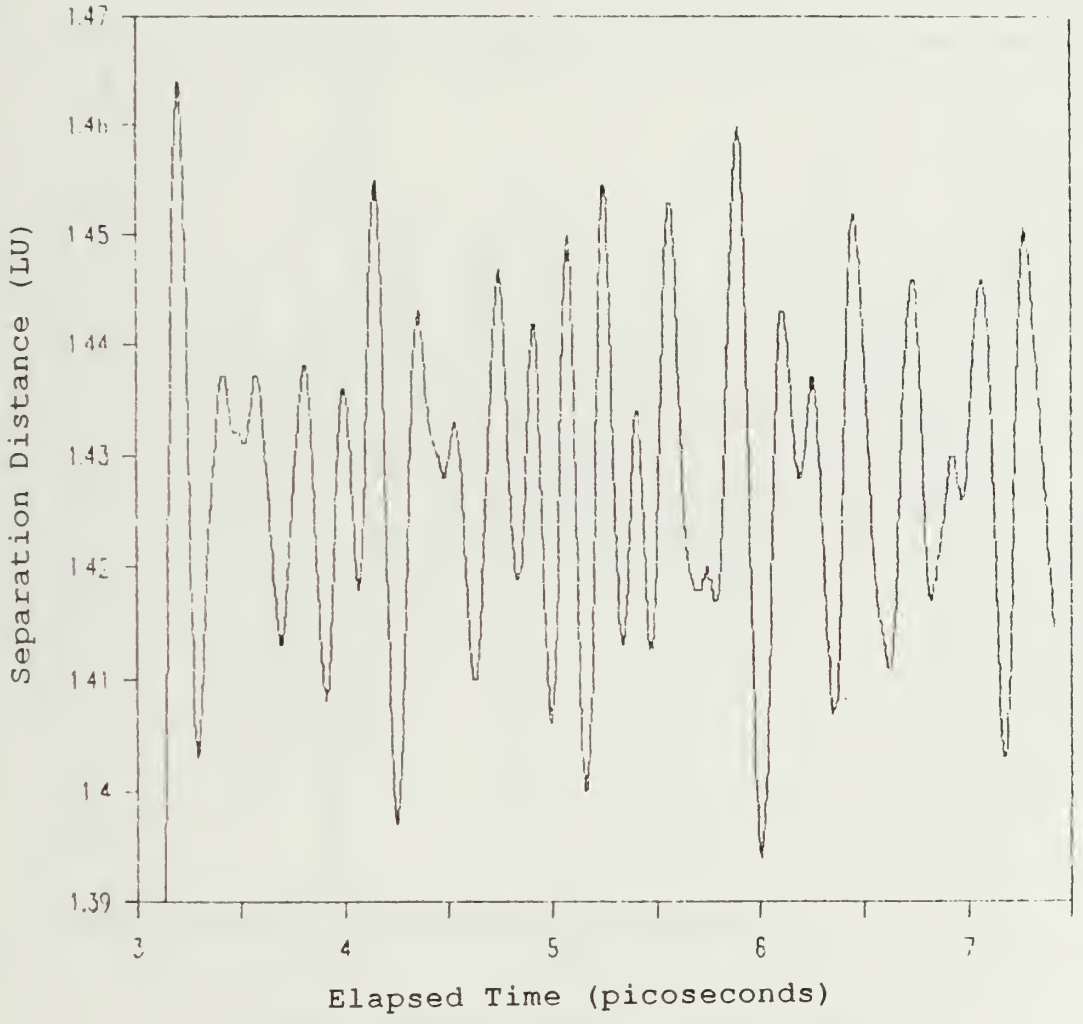

Figure B14. Oscillation of Atom 1 About the Body Centered Vacancy. The Plot Was Obtained Using the Alloy With No EE Losses.

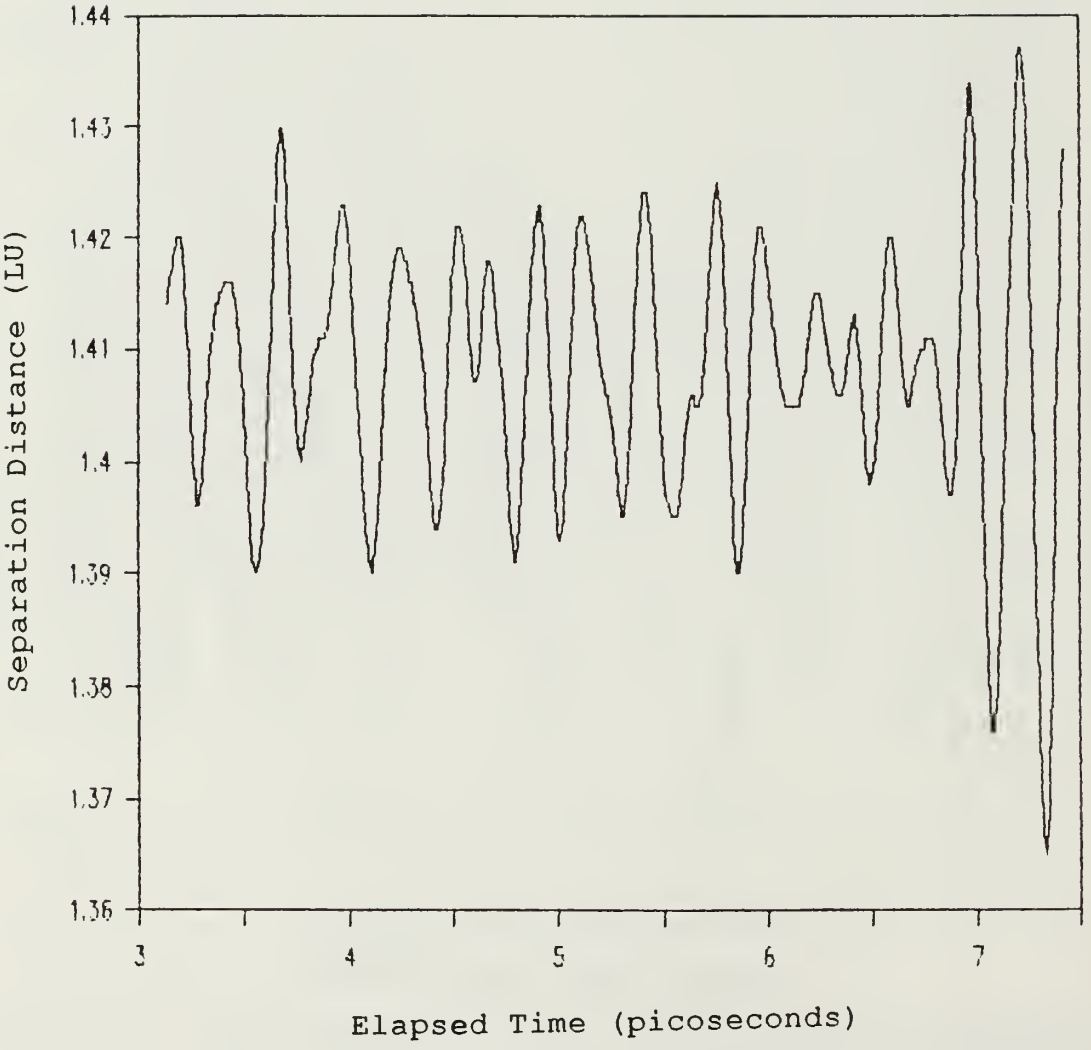

Figure B15. Oscillation of Atom 2 About the Body Centered Vacancy. The Plot Was Obtained Using the Alloy With No EE Losses.

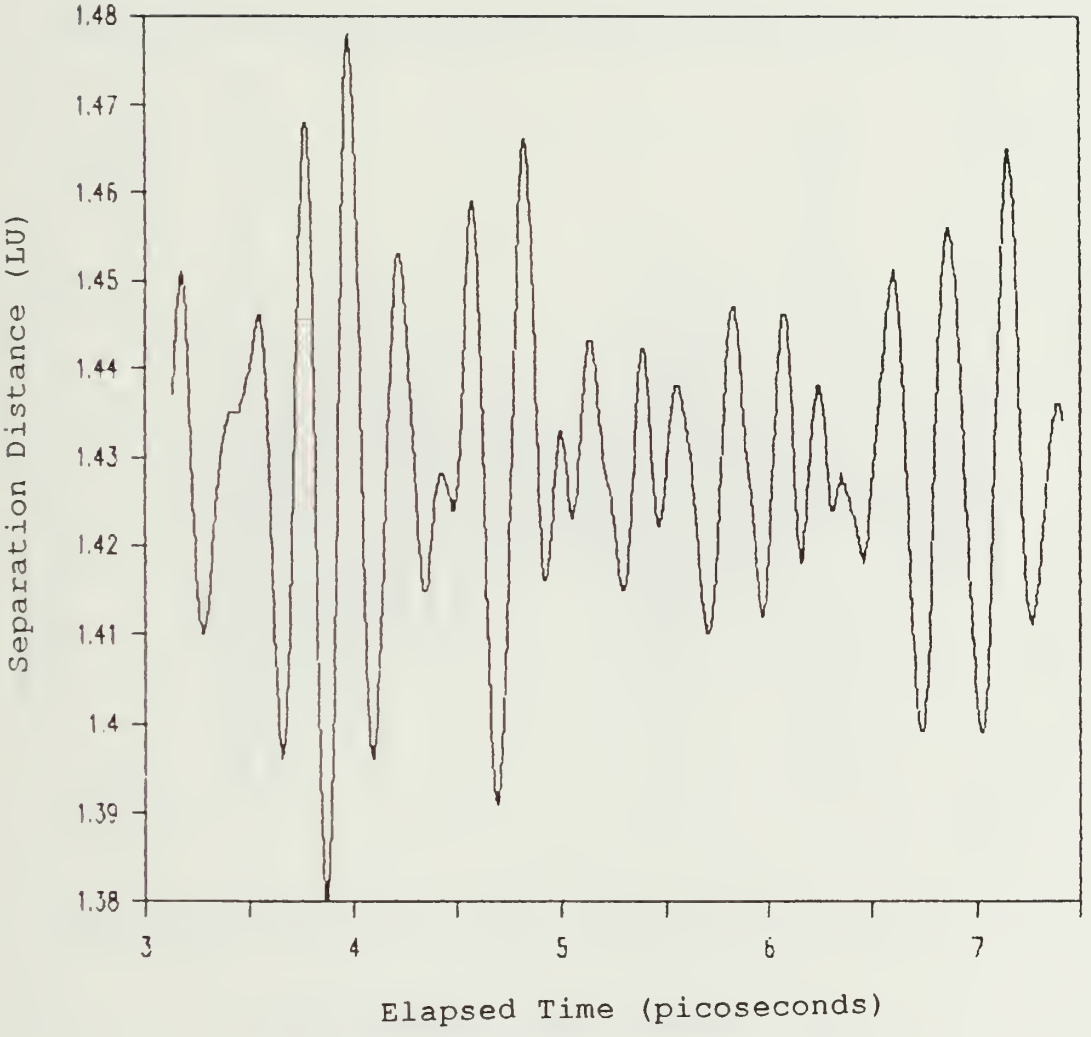

Figure B16. Oscillation of Atom 3 About the Body Centered Vacancy. The Plot Was Obtained Using the Alloy With No EE Losses.

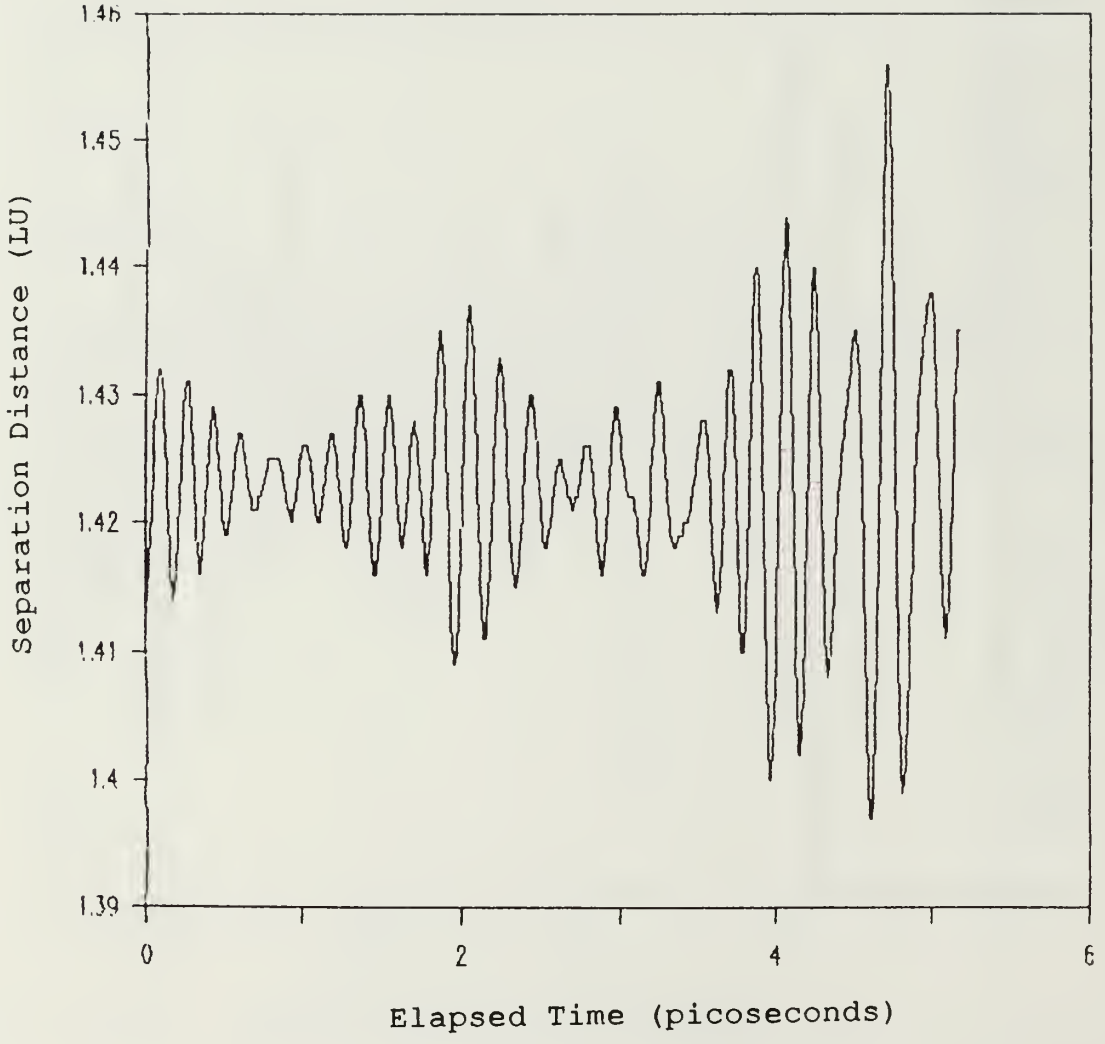

Figure B17. Oscillation of Atom 1 About the Body Centered Vacancy. The Plot Was Obtained Using Zr With No EE Losses.

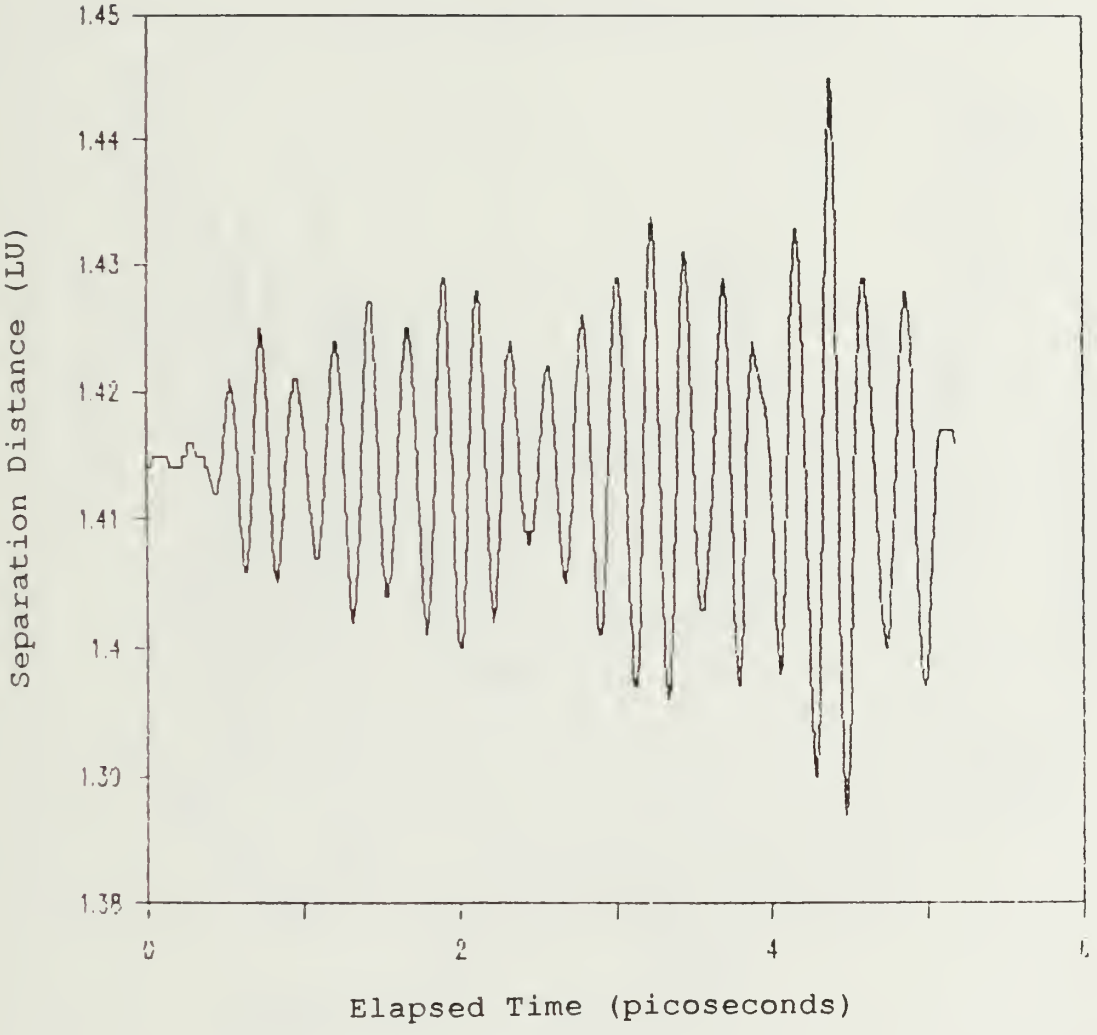

Figure B18. Oscillation of Atom 2 About the Body Centered Vacancy. The Plot Was Obtained Using Zr With No EE Losses.

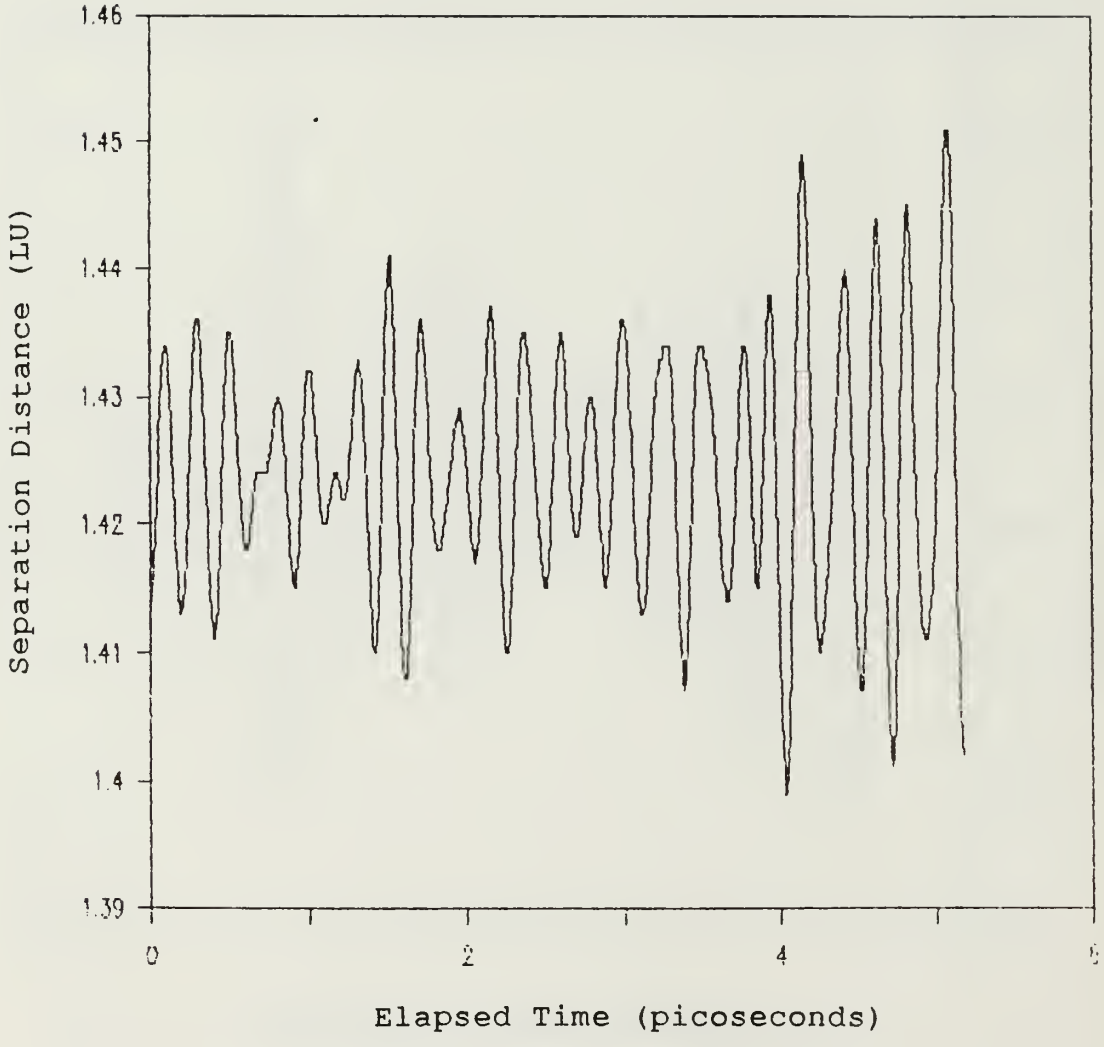

Figure B19. Oscillation of Atom 3 About the Body Centered Vacancy. The Plot Was Obtained Using Zr With No EE Losses.

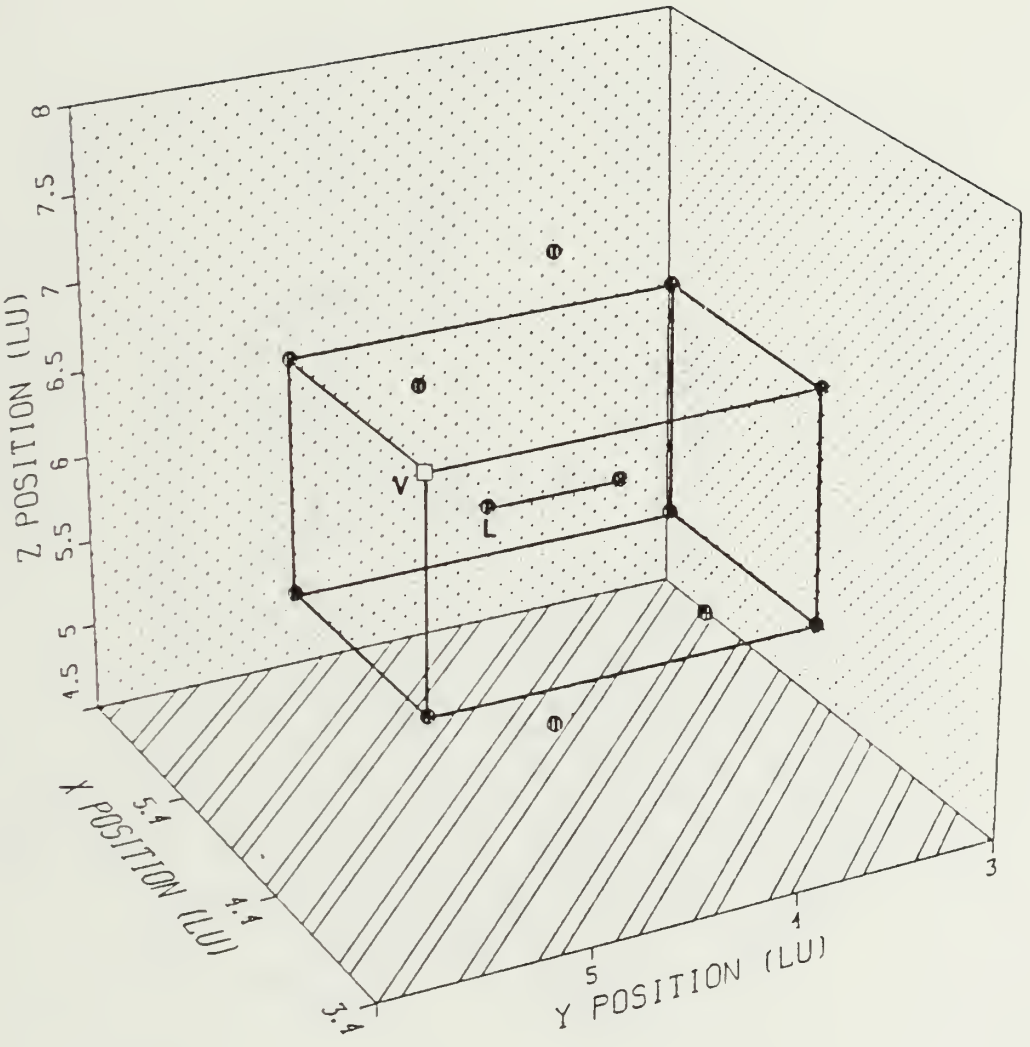

Figure B20. Vacancy-Interstitial Configuration for Recombination Case 1 Trials.

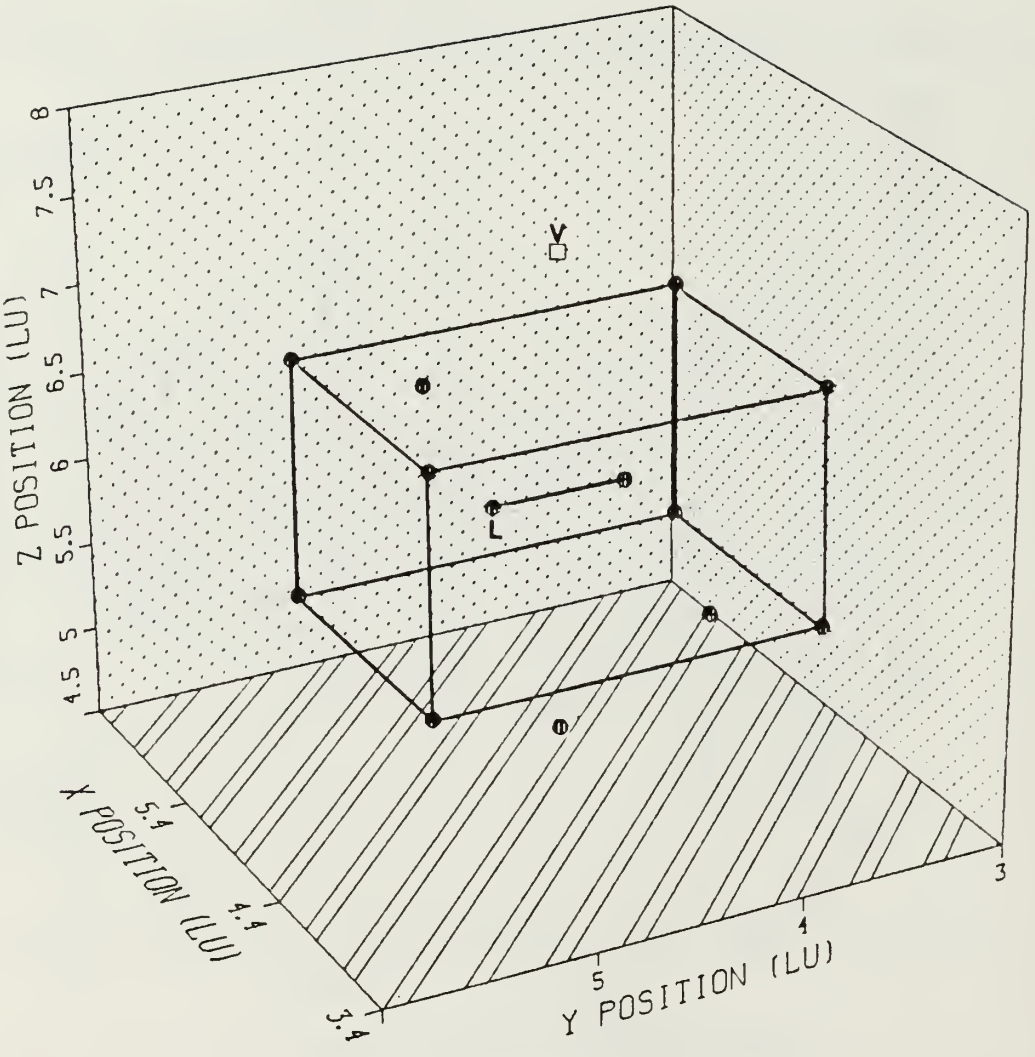

Figure B21. Vacancy-Interstitial Configuration for Recombination Case 2 Trials.

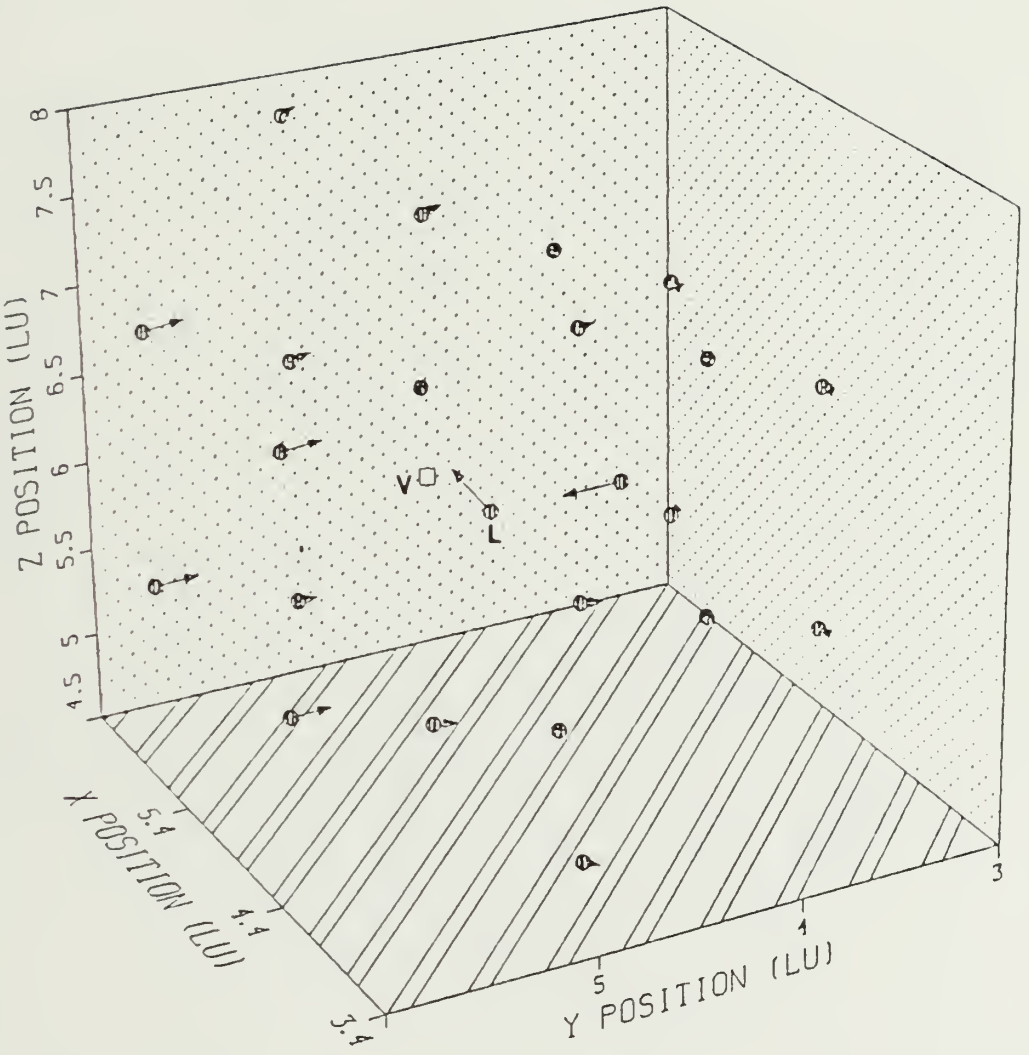

Figure B22. Sample Plot of the Atomic Displacements Produced as a Result of Vacancy-Interstitial Recombination.

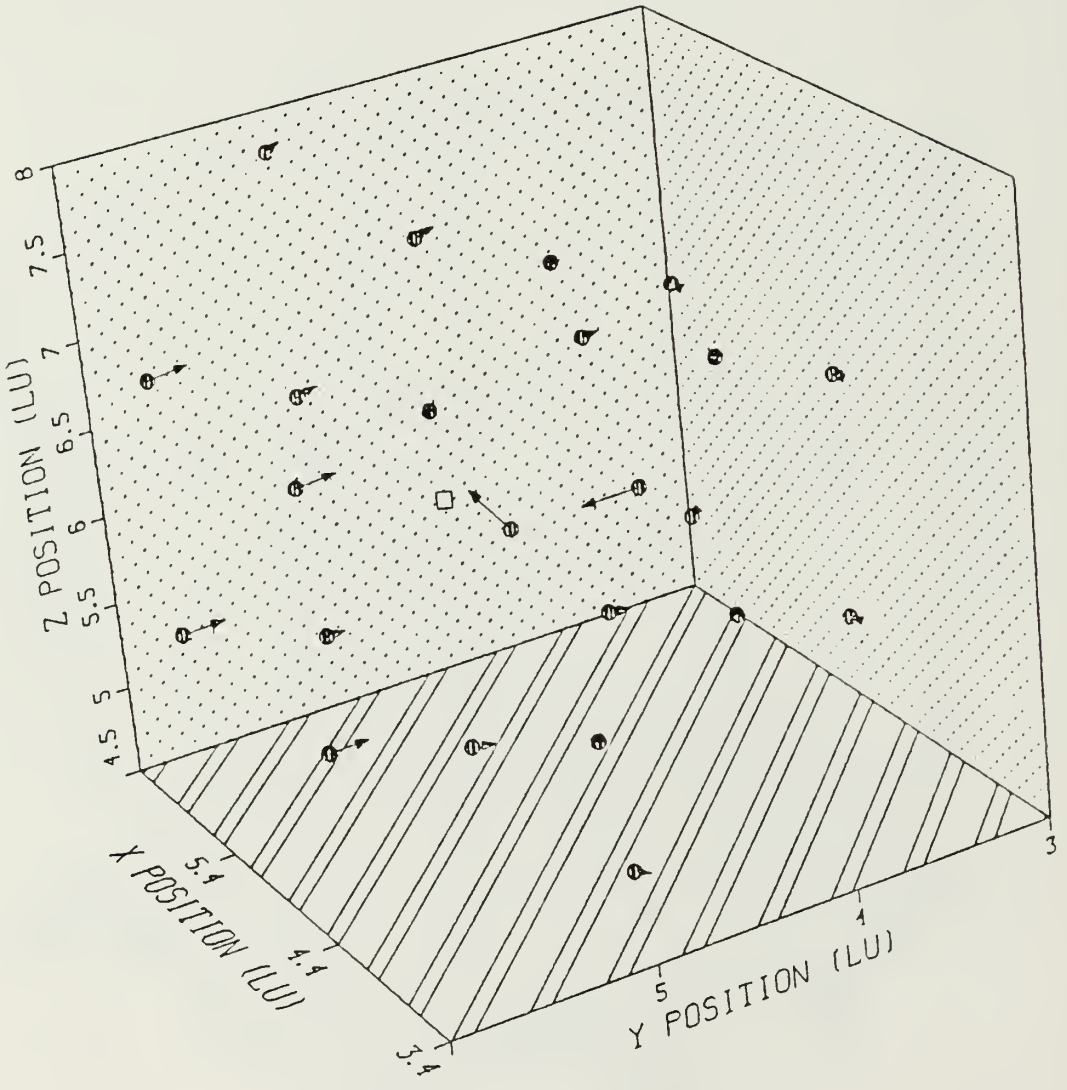

Figure B23. Atomic Displacements for Recombination Trial 2.

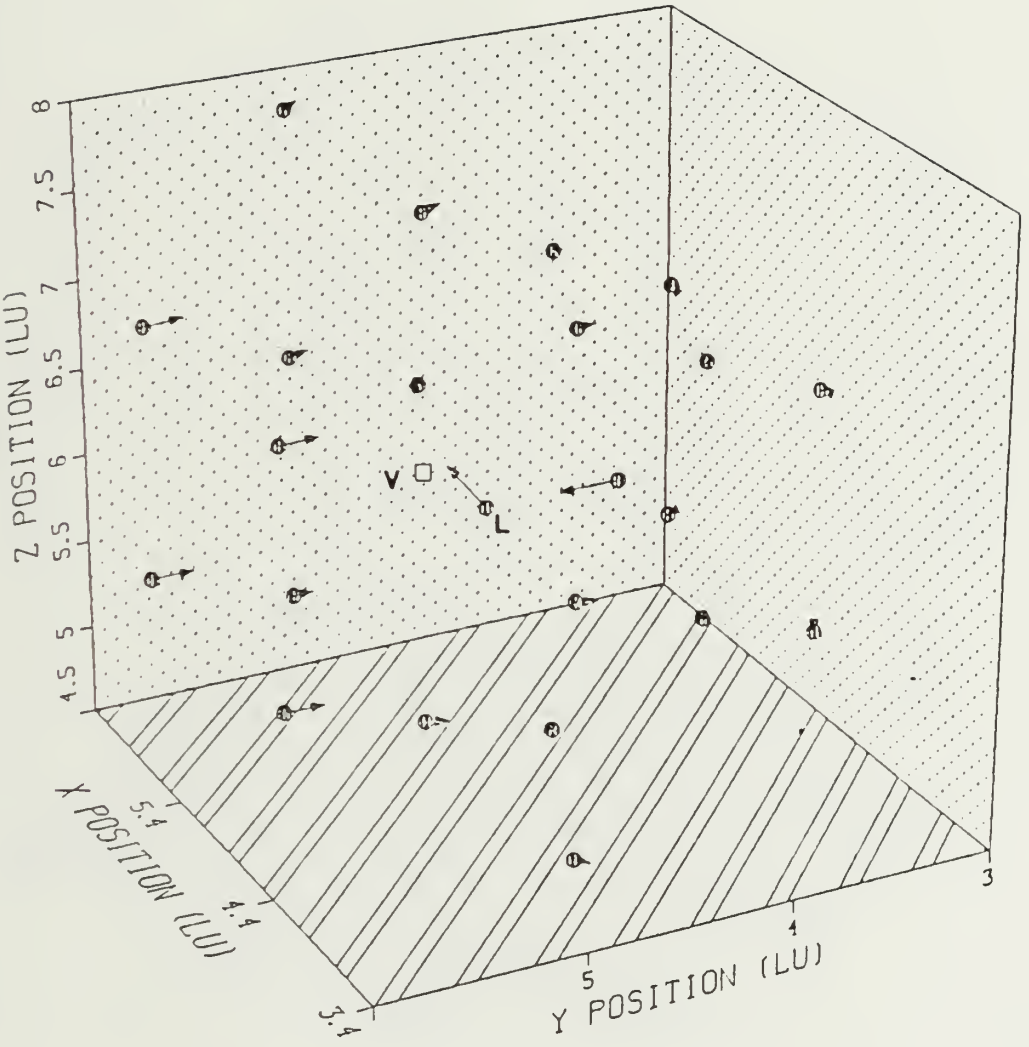

Figure B24. Atomic Displacements for Recombination Trial 14.

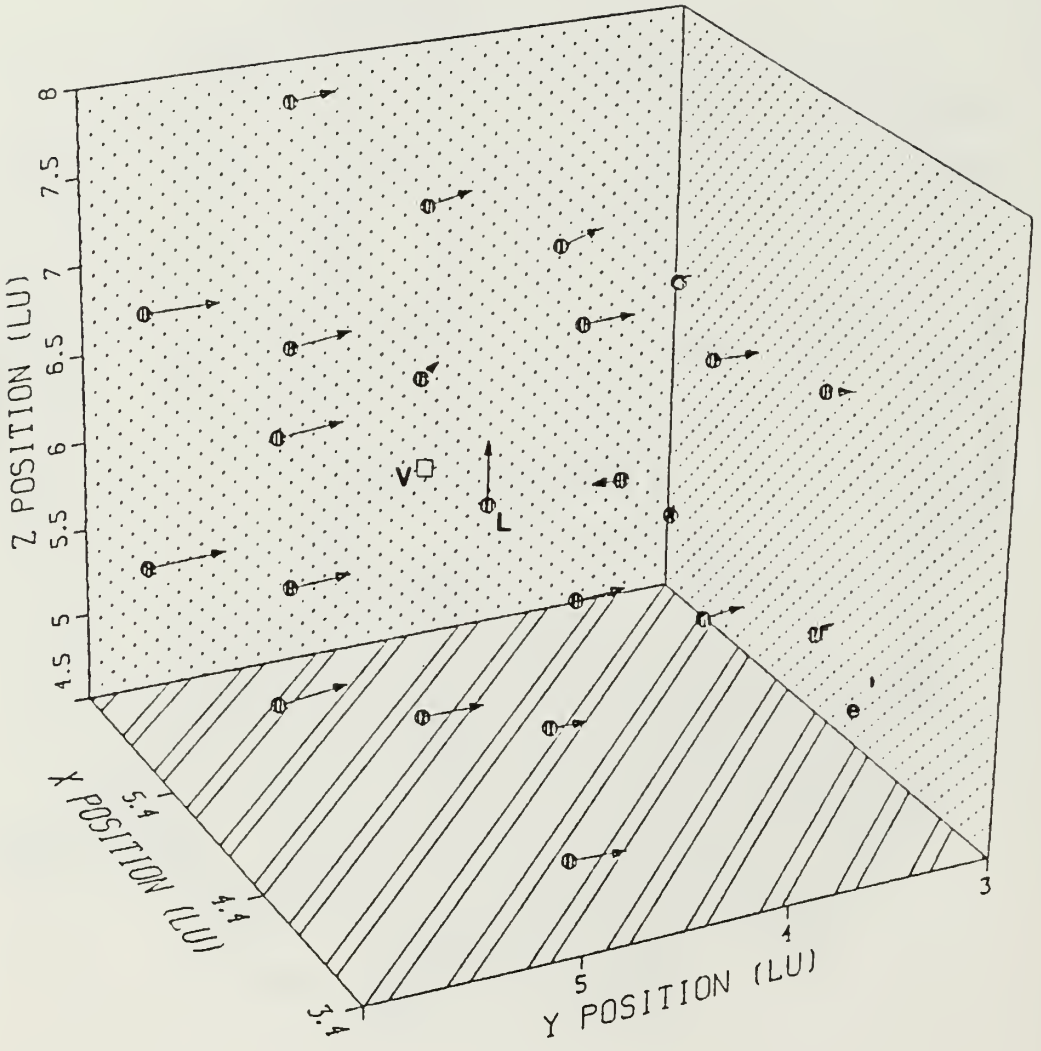

Figure B25. Atomic Displacements for Recombination Trial 1.

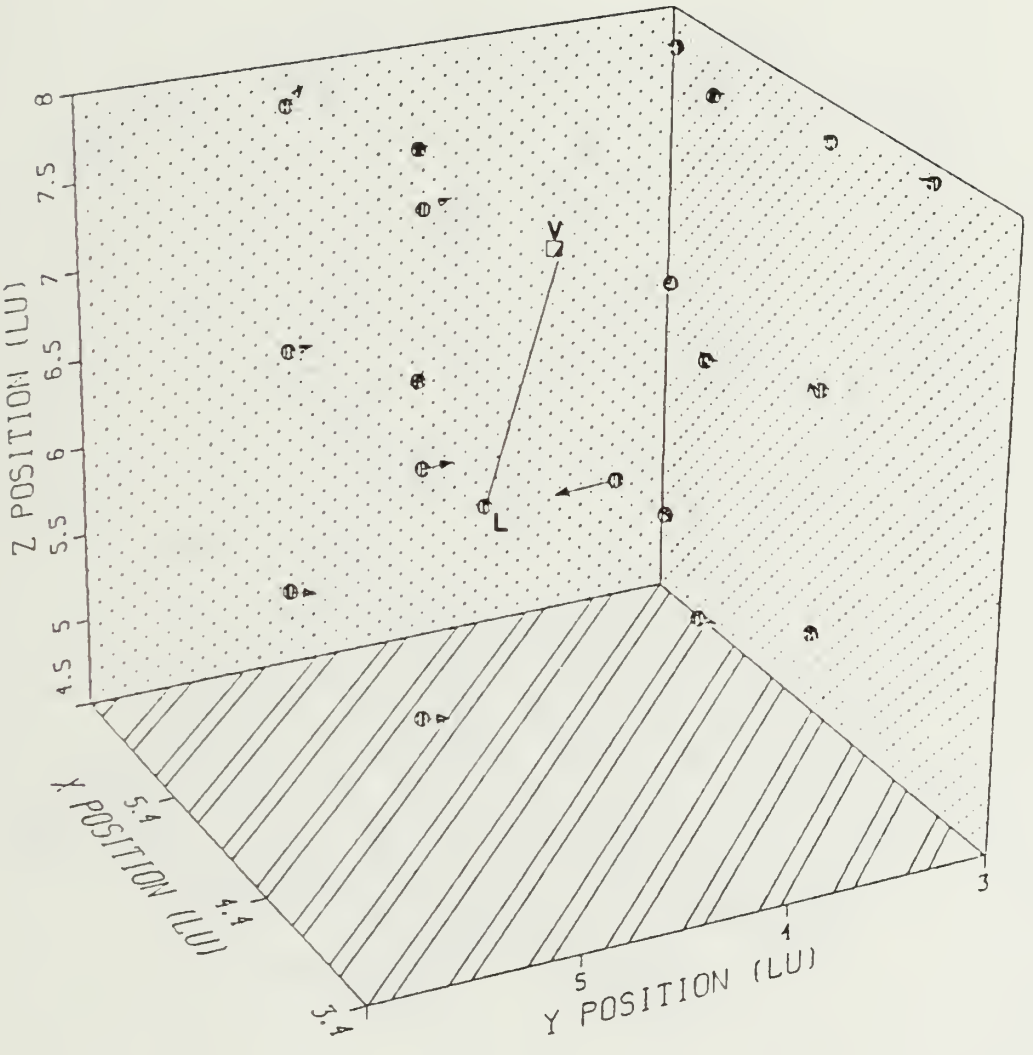

Figure B26. Atomic Displacements for Recombination Trial 20.

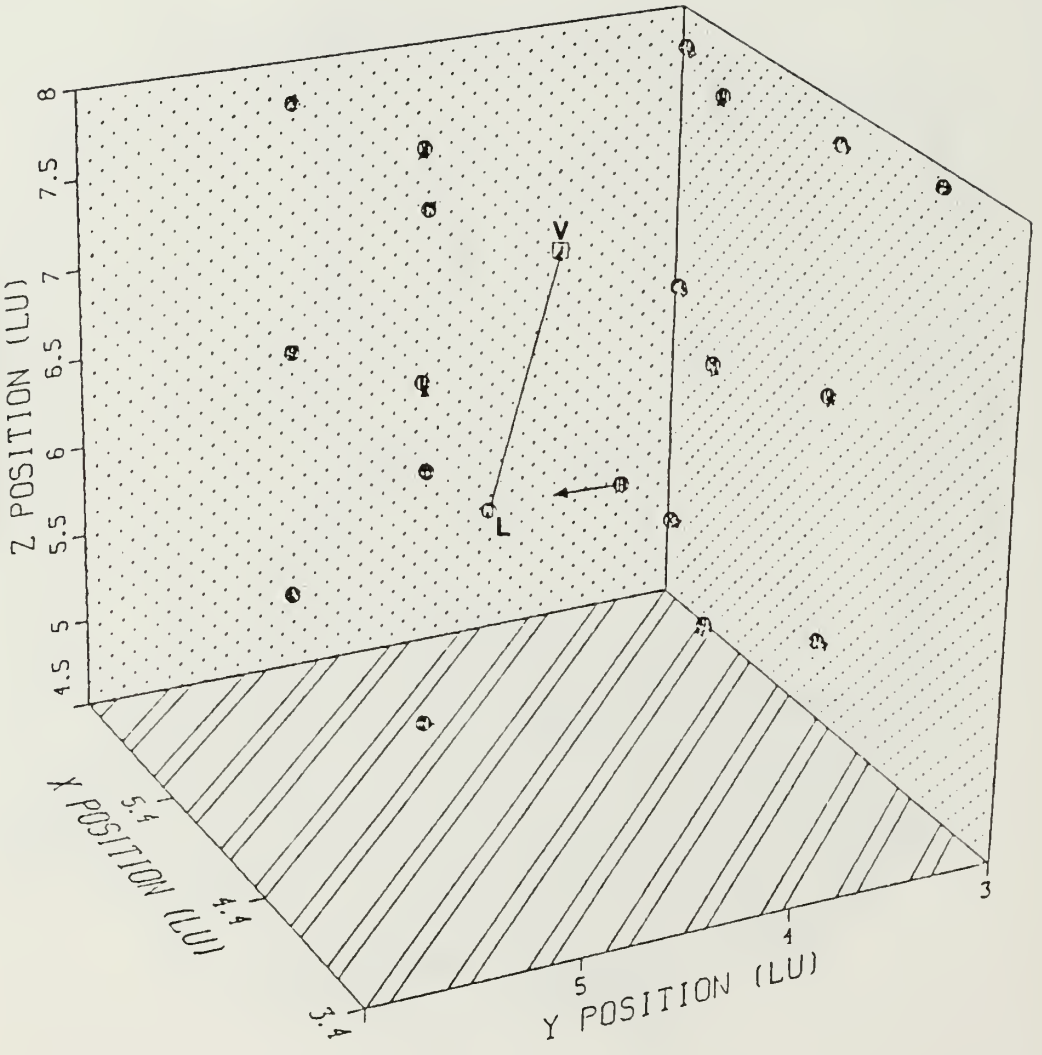

Figure B27. Atomic Displacements for Recombination Trial 21.

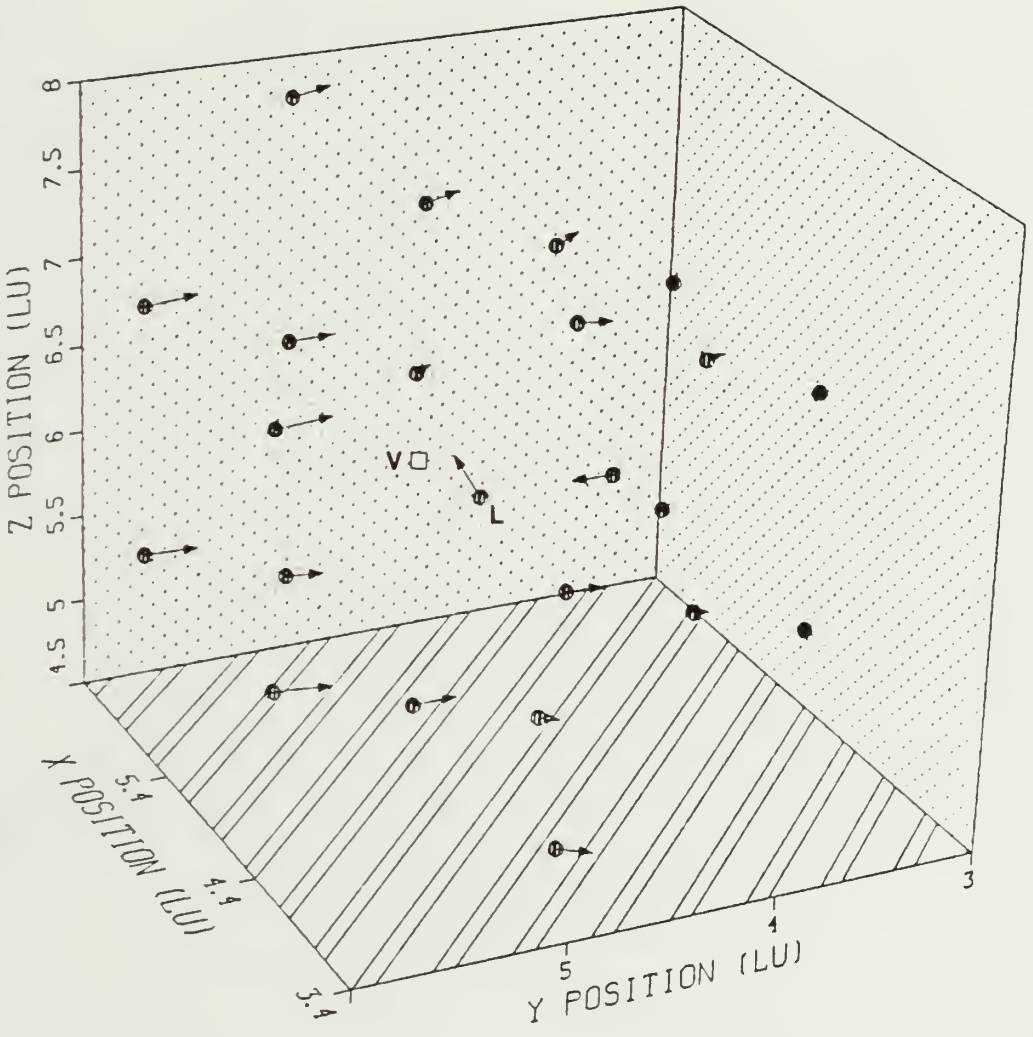

Figure B28. Atomic Displacements for Recombination Trial 5.

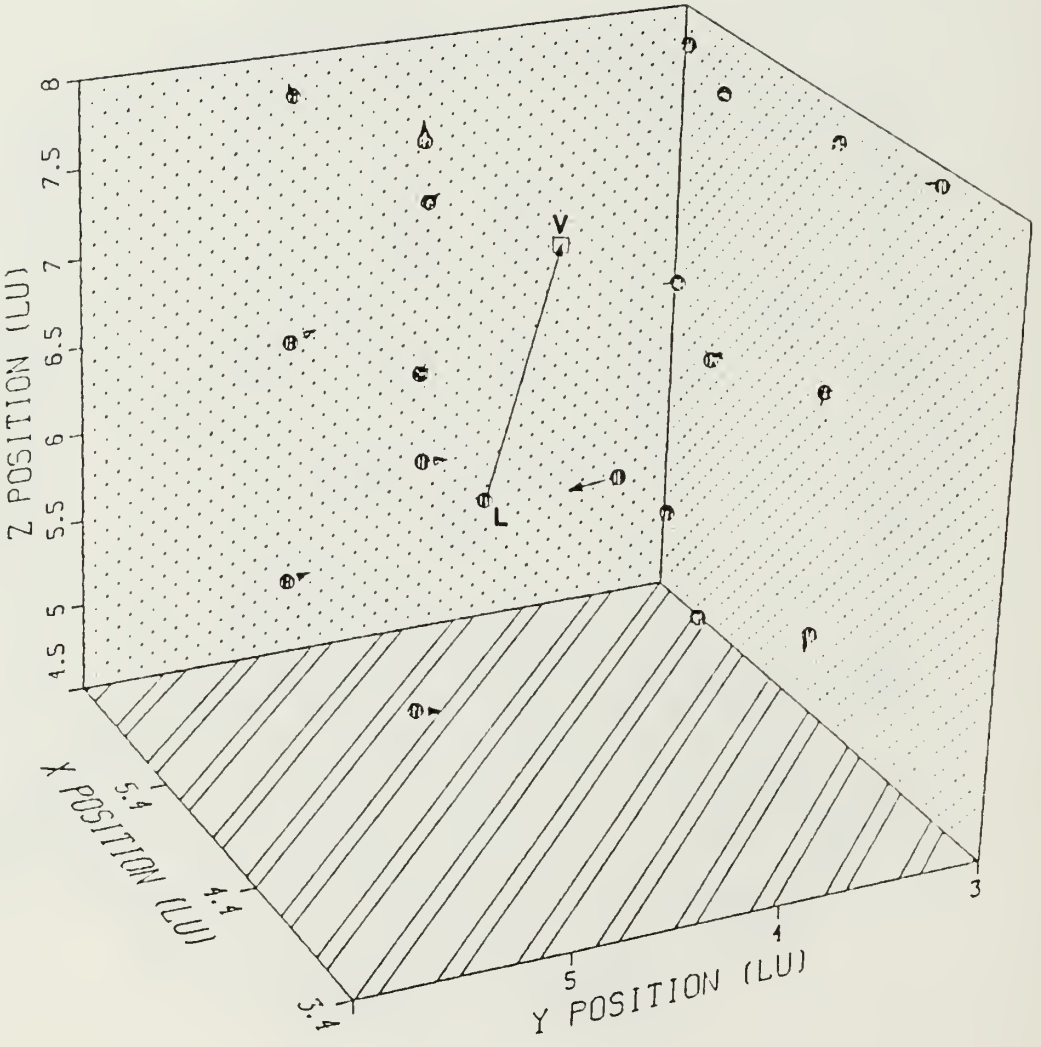

Figure B29. Atomic Displacements for Recombination Trial 23.

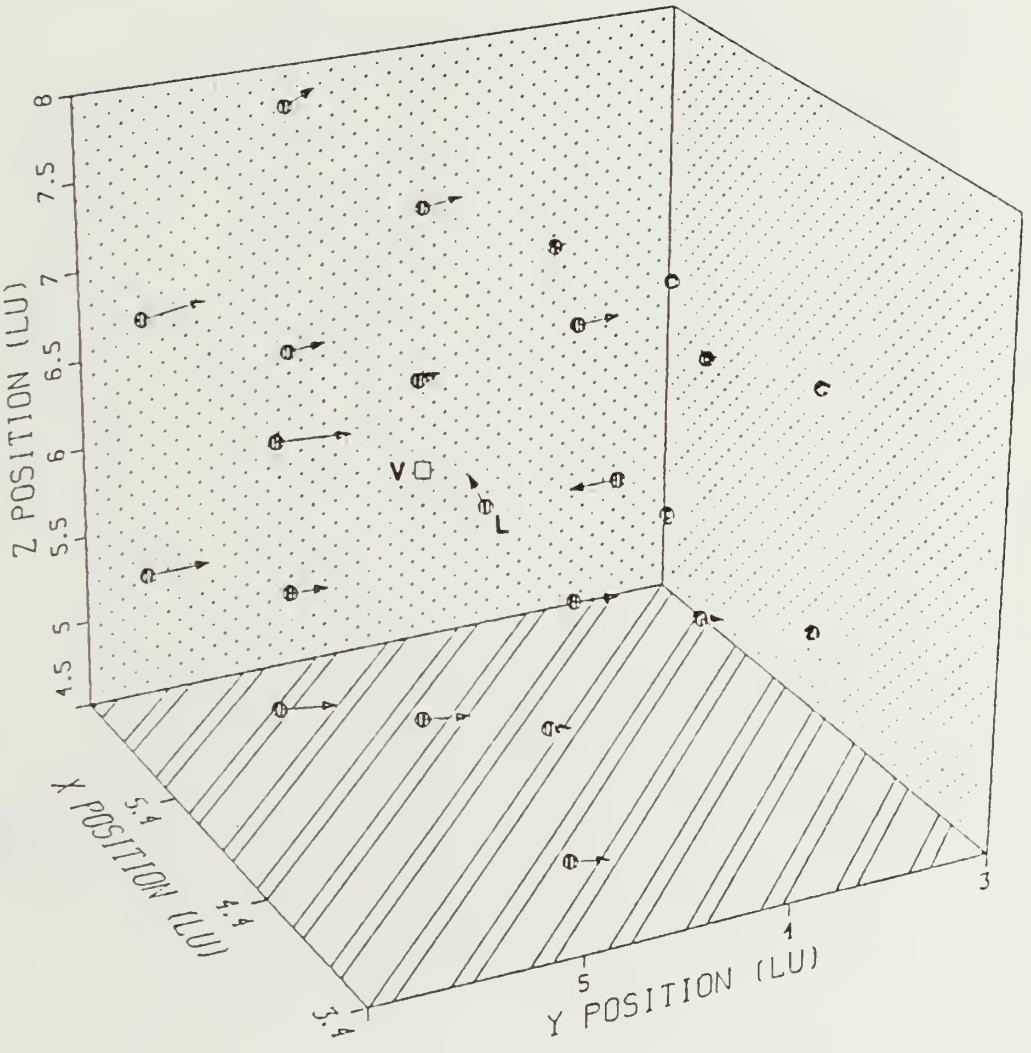

Figure B30. Atomic Displacements for Recombination Trial 17.

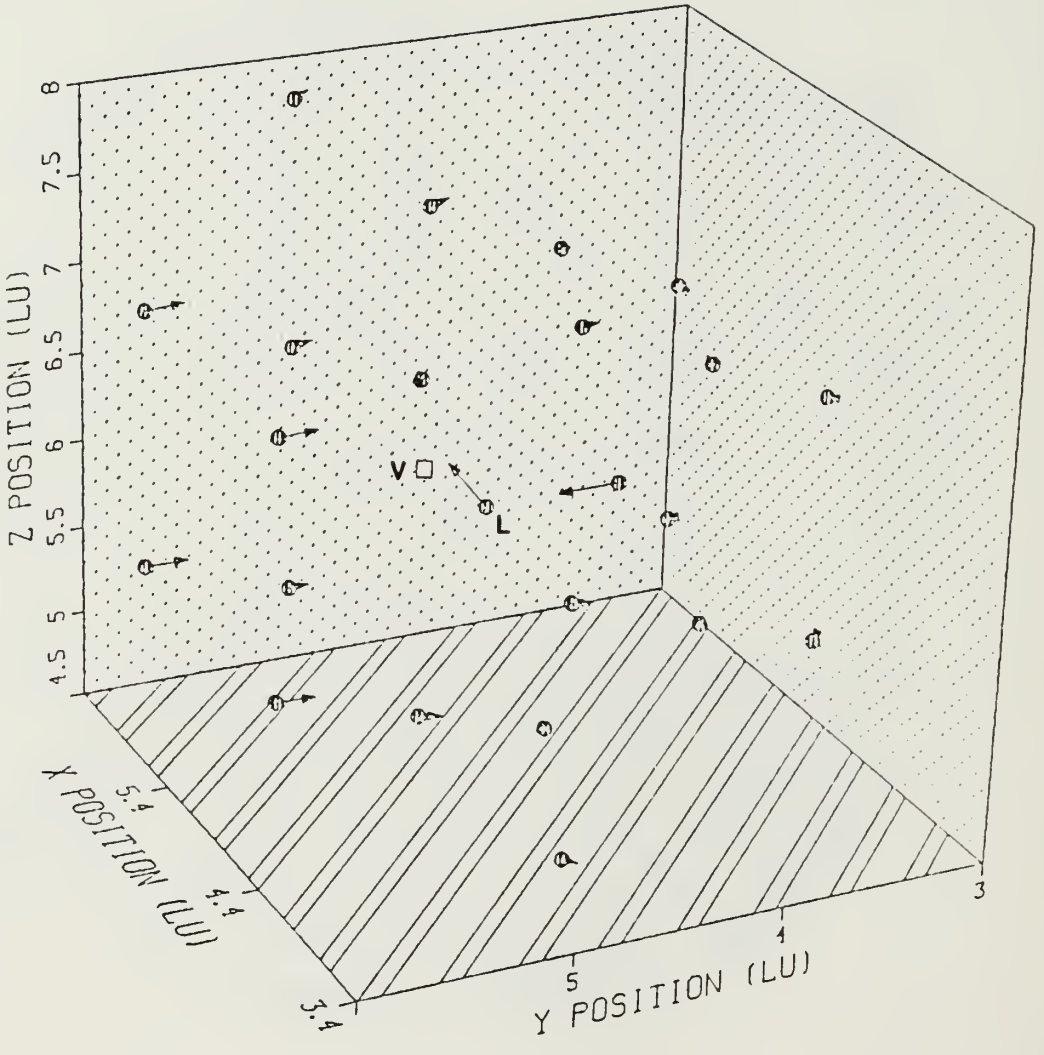

Figure B31. Atomic Displacements for Recombination Trial 18.

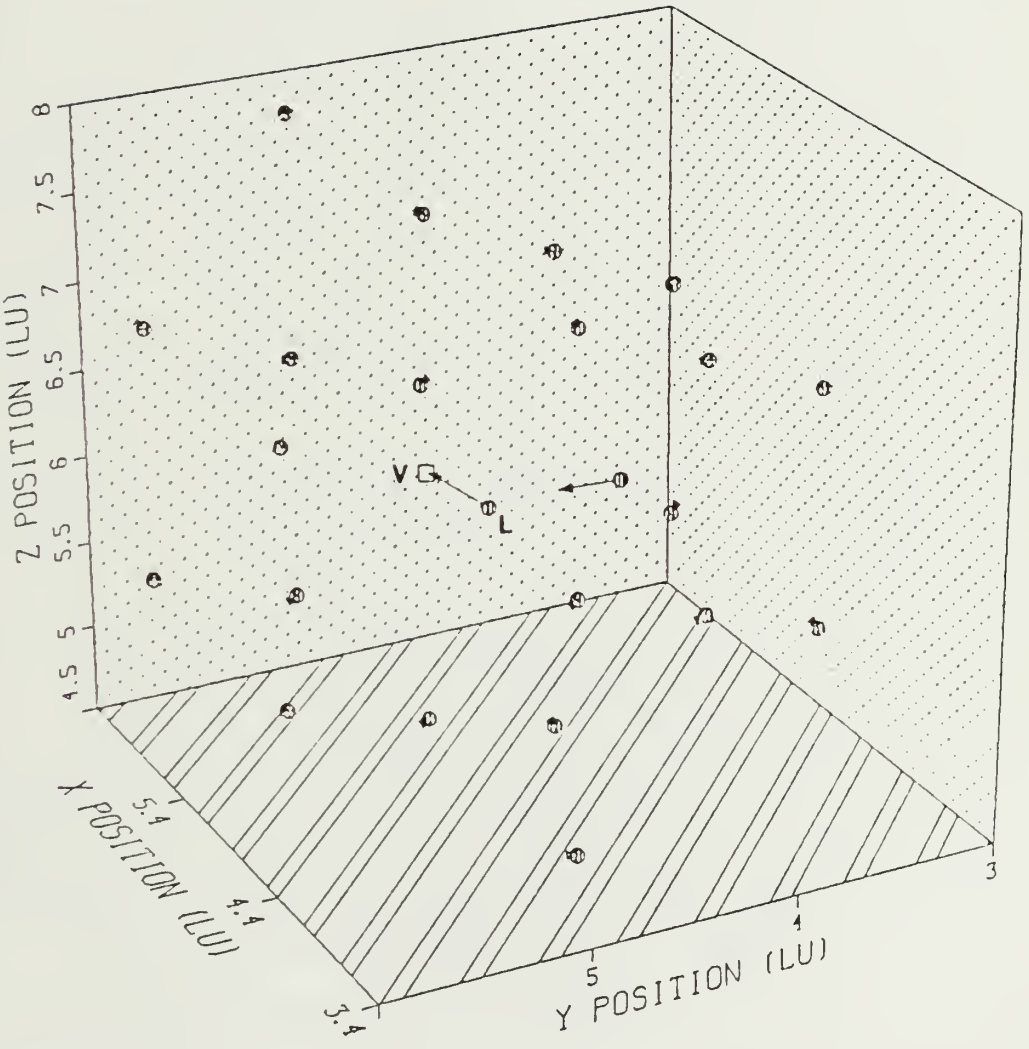

Figure B32. Atomic Displacements for Recombination Trial 16.

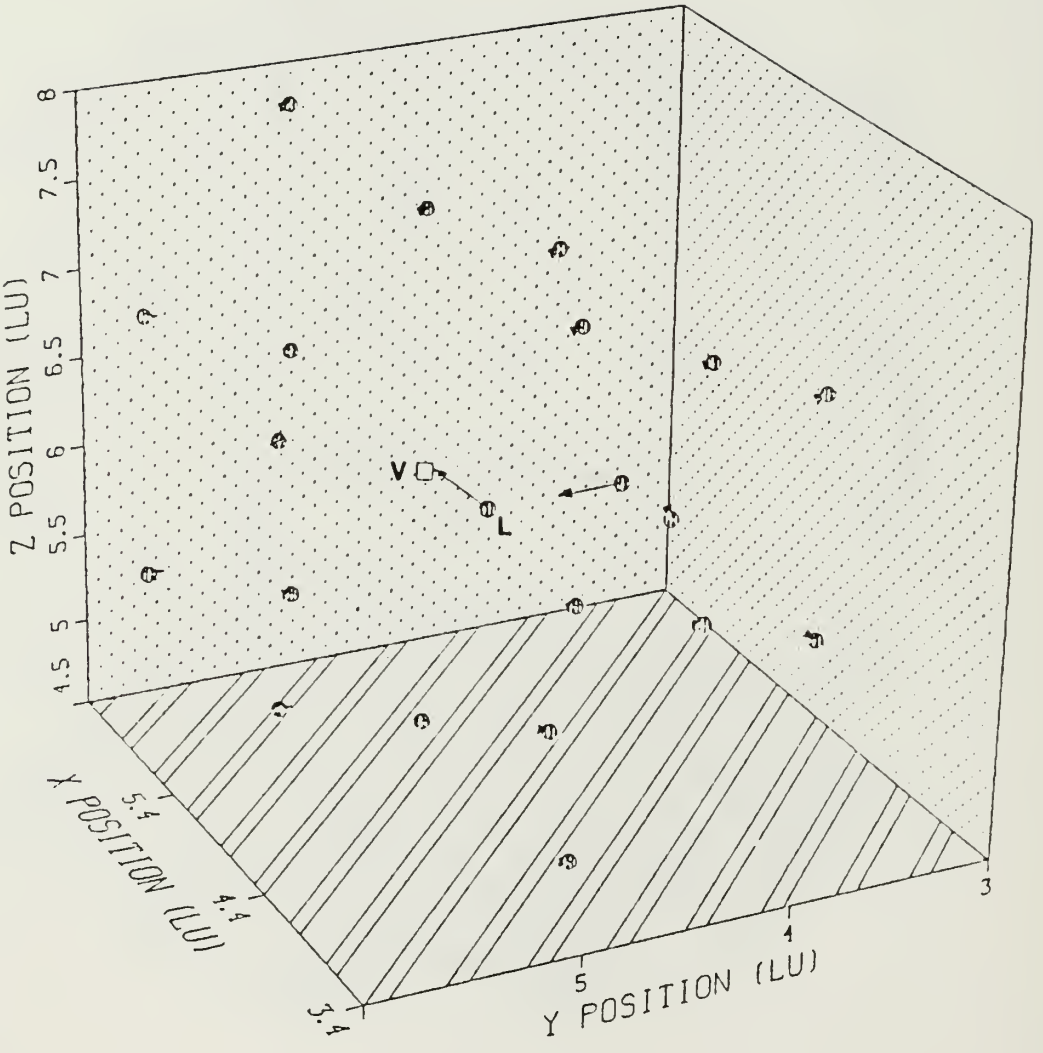

Figure B33. Atomic Displacements for Recombination Trial 36.

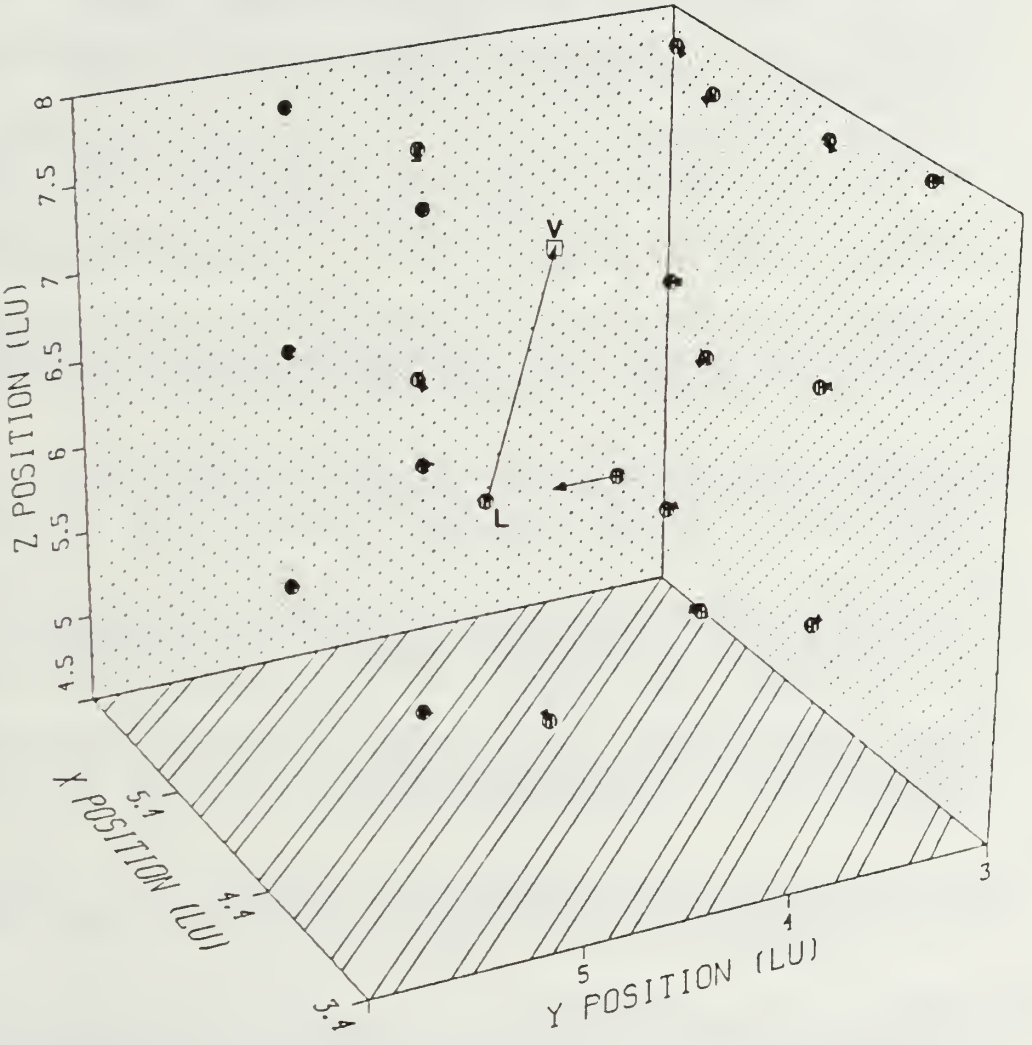

Figure B34. Atomic Displacements for Recombination Trial 33.

LIST OF REFERENCES

1. Howe, L.M., and Rainville, M.H., "A Study of the Irradiation Behaviour of Zr_3Al," Journal of Nuclear Materials, v. 68, pp. 215-234, March 1987.

2. Technical Information Center, Office of Public Affairs, Energy, Research and Development Administration, TID-26711-P1, Fundamental Aspects of Nuclear Reactor Fuel Elements, Olander, D.R., pp. 373-374, 1976.

3. Hausner, H.H., and Schumar, J.F., Nuclear Fuel Elements, Reinhold Publishing Corporation, NY, pp.338-339, 1959.

4. Seitz, F., "Radiation Effects in Solids," Physics Today, v. 5, pp. 6-9, June 1952.

5. Wigner, E.P., "Theoretical Physics in the Metallurgical Laboratories of Chicago," Journal of Applied Physics, v. 17, pp. 857-863, November 1946.

6. Brattain, W.H., and Pearson, G.L., "Changes in Conductivity of Germanium Induced by Alpha-Particle Bombardment," Physical Review, v. 80, p. 846, December 1950.

7. Siegel, S., "Effect of Neutron Bombardment on Order in the Alloy Cu_3Au," Physical Review, v. 75, Number 12, pp. 1823-1824, June 1949.

8. Howe, L.M., and Rainville, M.H., "Ion Bombardment of Ordered Zr_3Al," Radiation Effects, v. 48, pp.151-156, 1980.

9. Pedraza, D.F., "Amorphization of Intermetallic Compounds by Ion Bombardment," Materials Science and Engineering, v. 90, pp.69-80, 1987.

10. Pedraza, D.F., and Mansur, L.K., "The Effect of Point Defects on the Amorphization of Metallic Alloys During Ion Implantation," Nuclear Instruments and Methods in Physics Research, v. B16, pp. 203-211, 1986.

11. Agranovich, V.M., and Kirsanov, V.V., "Production of Radiation Defects by Collision Cascades in Metals," Modern Problems in Condensed Matter Sciences, v. 13, pp. 117-127, 1986.

12. Foster, A.H., Harder, J.M., and Bacon, D.J., "Computer Simulation of Interstitial Clusters in BCC and HCP Metals," Materials Science Forum, v. 15-18, pp.849-856, 1987.

13. Schober, H.R., "Single and Multiple Interstitials in FCC Metals," Journal of Physics F, v. 7, Number 7, pp.1127-1138, 1977.

14. Thompson, M.W., Defects and Radiation Damage in Metals, pp. 143-256, Cambridge University Press, NY, 1969.

15. Gibson, J.B., Goland, A.N., Milgram, M., and Vineyard, G.H., "Dynamics of Radiation Damage," Physical Review, v. 120, Number 4, pp. 1229-1252, 1960.

16. Howe, L.M., and Rainville, M.H., "The Nature of Irradiation-Produced Damaged Regions in Ordered Zr_3Al," Radiation Effects, v. 39, pp. 195-212, 1979.

17. Pedraza, D.F., "Mechanisms of the Electron Irradiation-Induced Amorphous Transition in Intermetallic Compounds," Journal of Materials Research, v.1, Number 3, pp. 425-441, 1986.

18. Huntington, H.B., "Creation of Displacements in Radiation Damage," Physical Review, v. 93, pp. 1414-1415, 1954

19. Young, W.J.S., Tucker, R.P., Cheng,B., and Adamson, R.B., "Precipitates in Zircaloy: Identification and the Effects of Irradiation and Thermal Treatment," Journal of Nuclear Materials, v. 138, pp. 185-195, 1986.

20. Pedraza, A.J., and Pedraza, D.F., "Microstructure and Dimensional Changes of Neutron-Irradiated Zirconium Alloys," Journal of Nuclear Materials, v. 108 and 109, p. 550, 1982.

21. Monti, A.M., "Vacancy and Small Vacancy Clusters in HCP Metals A static study," Materials Science Forum, v. 15-18, pp. 863-868, 1987.

22. United States Department of Commerce, National Bureau of Standards Special Publication 317, v. 1, Fundamental Aspects of Dislocation Theory, pp. 273-283, Government Printing Office, Washington, DC 1970.

23. Fletcher, R., and Reeves, C.M. "Function Minimization by Conjugate Gradients," Computer Journal, v. 7, pp. 149-154, 1964.

24. Savino, E.J., and Perrin, R.C., "The Morphology of Planar Vacancy Aggregates in Copper," Journal of Physics F, v. 4, pp.1889-1897, 1974.

25. Harrison, D.E., Gay, W.L., and Effron, H.M., "Algorithm for the Calculation of the Classical Equations of Motion of an N-Body system," Journal of Mathematical Physics, v. 10, Number 7, pp. 1179-1184, 1969.

26. Lindhard, L., and Scharff, M., "Energy Dissipation by Ions in the keV Region," Physical Review, v. 124, p. 128, 1961.

27. Harrison, D.E., and Jakas, M.M., "Simulation of the Atomic Collision Cascade," Radiation Effects, v. 99, pp. 153-169, 1986.

28. Chemical Rubber Company, Handbook of Chemistry and Physics, 54th ed., CRC Press, 1973.

29. Miller, G.L., Zirconium, pp. 354-357, Academic Press Inc., 1957.

30. Pearson, W.B., Handbook of Lattice Spacings and Structures of Metals, v. 1, pp.391, 888, Pergamon Press, NY, 1967.

31. Torrens, I.M., Interatomic Potentials, Academic Press Inc., NY, 1972.

32. Harrison, D.E., "Application of Molecular Dynamics Simulations to the Study of Ion-Bombarded Metal Surfaces," Critical Reviews in Solid State and Materials Science, v. 14, pp. S1-S78, 1988.

INITIAL DISTRIBUTION LIST

1.	Defense Technical Information Center Cameron Station Alexandria, Virginia 22304-6145	2
2.	Library, Code 0142 Naval Postgraduate School Monterey, California 93943-5002	2
3.	Naval Postgraduate School Department of Physics Monterey, California 93943-5002 Attn: Department Chairman, Code 61WH	2
4.	Naval Postgraduate School Department of Physics Monterey, California 93943-5002 Attn: Dr. Roger Smith, Code 61SM	2
5.	Oak Ridge National Laboratory Post Office Box 2008 Oak Ridge, Tennessee 37831-6376 Attn: Dr. Dora Pedraza, Bldg. 5500	2
6.	Lieutenant Vito Menzella, USN 95 Wilson Street Little Ferry, New Jersey 07643	2

DUDLEY
OL
3-5002

Thesis
M4855
c.1

Menzella
Atomic relaxation and
vacancy-interstitial
recombination in Zr and
Zr_3Al.

Thesis
M4855
c.1

Menzella
Atomic relaxation and
vacancy-interstitial
recombination in Zr and
Zr_3Al.

AMERICAN BINDERY
TOPEKA KANSAS

thesM4855
Atomic relaxation and vacancy-interstiti
3 2768 000 81544 3
DUDLEY KNOX LIBRARY